remote sensing

MDPI

Article

Multi-Criteria Assessment of Urban Thermal Hotspots: A GIS-Based Remote Sensing Approach in a Mediterranean Climate City

Javier Sola-Caraballo [1,*], Antonio Serrano-Jiménez [2], Carlos Rivera-Gomez [1] and Carmen Galan-Marin [1]

[1] Departamento de Construcciones Arquitectónicas I, Escuela Técnica Superior de Arquitectura, Universidad de Sevilla, Avda. Reina Mercedes, 2, 41012 Seville, Spain; crivera@us.es (C.R.-G.); cgalan@us.es (C.G.-M.)
[2] Departamento de Construcciones Arquitectónicas, Escuela Técnica Superior de Arquitectura, Universidad de Granada, Campo del Principe, sn, 18071 Granada, Spain; serranojimenez@ugr.es
* Correspondence: jdesola@us.es; Tel.: +34-954-556-59

Abstract: One of the most significant urban challenges focuses on addressing the effects of urban overheating as a consequence of climate change. Several methods have been developed to characterize urban heat islands (UHIs); however, the most widely used involve complex planning, huge time consumption, and substantial human and technical resources on field monitoring campaigns. Therefore, this study aims to provide an easily accessible and affordable remote sensing method for locating urban hotspots and addresses a multi-criteria assessment of urban heat-related parameters, allowing for a comprehensive city-wide evaluation. The novelty is based on leveraging the potential of the last Landsat 9 satellite, the application of kernel spatial interpolation, and GIS open access data, providing very high-resolution land surface temperature images over urban spaces. Within GIS workflow, the city is divided into LCZs, thermal hotspots are detected, and finally, it is analyzed to understand how urban factors, such as urban boundaries, building density, and vegetation, affect urban scale LST, all using graphical and analytical cross-assessment. The methodology has been tested in Seville, a representative warm Mediterranean city, where variations of up to 10 °C have been found between homogeneous residential areas. Thermal hotspots have been located, representing 11% of the total residential fabric, while results indicate a clear connection between the urban factors studied and overheating. The conclusions support the possibility of generating a powerful affordable tool for future research and the design of public policy renewal actions in vulnerable areas.

Keywords: urban overheating; land surface temperature; local climate zones; urban density; thermal hotspots; outdoor environmental comfort

check for updates

Academic Editor: Janet Nichol

Received: 30 October 2024
Revised: 2 January 2025
Accepted: 8 January 2025
Published: 10 January 2025

Citation: Sola-Caraballo, J.; Serrano-Jiménez, A.; Rivera-Gomez, C.; Galan-Marin, C. Multi-Criteria Assessment of Urban Thermal Hotspots: A GIS-Based Remote Sensing Approach in a Mediterranean Climate City. *Remote Sens.* **2025**, *17*, 231. https://doi.org/10.3390/rs17020231

Copyright: © 2025 by the authors. Licensee MDPI, Basel, Switzerland. This article is an open access article distributed under the terms and conditions of the Creative Commons Attribution (CC BY) license (https://creativecommons.org/licenses/by/4.0/).

1. Introduction

Global warming's acceleration [1] prompts urgent bioclimatic urban regeneration strategies [2], particularly in warm regions and cities as they project to host 68% of the global population by 2050 [3,4]. Thus, research must prioritize efficient urban management, emphasizing urban comfort [5,6] and sustainable planning [7,8], offering, therefore, guidelines and methodologies for public specialists and policymakers. In this sense, the literature has widely studied the urban heat island (UHI) phenomenon [9,10], which occurs mainly during the night. However, recent studies are focusing on diurnal urban heat, as during the day the temperatures and cooling consumption peaks are reached [5,11].

Classical UHI studies involve high-resource field campaigns [12–14] to characterize heat distribution, making it difficult to sample the entire city. These studies typically focus

on air temperature (AT) in the urban canopy layer [15,16]; however, recent studies are analyzing land surface temperature (LST) and assessing the surface urban heat island (SUHI). Infrared studies [17] and remote sensing techniques [18] based on satellite acquisition are crucial to analyze SUHI, providing quick and effective identification of an area of interest (AOI), with high-resolution images of an entire city or regional zone at the same time.

It is important to clarify that LST is an indirect measure that highly depends on variables such as spatial resolution and the material properties of each surface. This can create limitations for studying effective air temperature or thoroughly evaluating thermal comfort. On the contrary, remote sensing obtains LST data instead of AT; although there is a discrepancy between them [19], recent research has found a certain correlation [20,21], mostly with comfort as it is highly influenced by mean radian temperature [22]. Despite that, numerous previous studies support it as a useful tool for studying the thermal and climatic performance of the city [17], as it can capture large areas and be compared with many other interrelated parameters. Thus, understanding its limitations and potential, it becomes a powerful tool for characterization and diagnosis at the city scale [23]. Specifically, this research focuses on the Landsat 9 satellite, launched by NASA and USGS [24]. Thermal infrared sensors provide LST images with an accuracy of 0.4–1.98 K [25].

The urban climate literature addresses several aspects that strongly influence the urban microclimate [26]. Among these, it is worth noting the widespread concept of the local climate zone (LCZ) [27,28]. This classification, widely tested in previous studies [29], helps to establish solid correlations between urban typologies and climate performance [30,31], which also affects directly buildings' cooling energy [32,33]. Other studies have focused on the land use–land cover (LULC) classification [34] and its relationship with LST [35], while others have established automatic machine-learning UHI predictions based on LULC [36]. Regarding this, the Copernicus' CORINE programme has developed a very detailed open-access LULC classification map [37], whose results are useful to urban research. Additional studies have substantiated considerably other several parameters crucial to understand urban heat performance [38]. The Sky View Factor (SVF) index [39,40] has been found to be crucially related to the potential of an area to receive sun radiation and dissipate it later [41,42]. Other relevant parameters include green structures and the Normalized Difference Vegetation Index (NDVI) [43,44]. Vegetation can reduce AT [45], but also protect from direct solar radiation, influencing LST [46]. Furthermore, soils and pavement materials have been found relevant to LST and so urban climate [14,35].

To manage remote sensing data within all these urban parameters on large scales involves extensive processing, and the geographical information system (GIS) is specially designed to face these skills [41,47]. This research uses Quantum GIS (QGIS) version 3.34.6 [48], an open-source software, widely used which has been tested by several studies [49,50]. Some of them highlight the usefulness of remote sensing in GIS tools for urban climate and UHI evaluation [51,52]. Other recent studies used GIS to combine LST data with urban parameter analysis to obtain socioeconomic and fuel-energy assessments [53,54], mapping vulnerability urban maps. Other research combined most of the previous fields [38,50,55] to focus specifically on the search for hotspots or particularly warm areas in the city [56,57], emphasizing the potential of these resources as diagnostic tools.

After this background analysis, several gaps have been observed in the literature. Many studies provide UHI characterization approaches [13,14], but most are resource-intensive or can become difficult to address. Other approaches are based on automatized algorithms for spatial classification [25,34,58]; however, this can result in low accuracy for detailed urban studies. Most of the research uses thermal images with large-scale and low-resolution images [20,50,59,60], which is useful for regional large-scale studies or for

assessing SUHI temporal evolution. However, the low spatial resolution fails to properly address diagnostics within the urban fabric at the public space and streets scale. Other research estimates SVF but without considering trees [61], which have a considerable effect of overestimation of solar radiation in urban canyons. Finally, it has been noted that many studies do not provide detailed affordable methodologies or guidelines. This hinders replicability by technicians and policymakers who are not familiar with remote sensing. If these methods are not precise, they cannot be properly reproduced and, therefore, are not implemented in urban policies, resulting in a lost opportunity to enhance the climate resilience of many warm cities.

Based on the above, the novelty of this research is to raise an open-access and replicable urban-scale method which, by addressing the role of the urban environment, provides optimized images and post-analysis, allowing for better identification of urban thermal hotspots, as well as their behaviour and performance according to urban features. In this way, this methodology provides essential tools to address the scientific issues necessary for the identification and characterization of urban thermal hotspots. Firstly, the LST of an entire city is obtained at a very high resolution, thanks to thermal satellite images and statistical rescaling. Although LST is not equivalent to AT, according to the literature, it provides valuable information. Also, due to its fine scale, it encompasses public space and the distribution of heat in the city. Additionally, the cross-multifactor analysis (land use, building density, vegetation, etc.) allows for the understanding of parameters related to thermal performance. The analysis examines typical values according to the literature, identifies relationships, and thus provides insights into the causes and diagnoses of the mentioned hotspots.

Thus, this novel method, by formulating specific research questions, and answering them with affordable technical approaches, provides a powerful diagnostic tool for identifying particularly hot areas, as well as improving the understanding of urban overheating and its causes, and offering a glimpse of possible future renovations, all focused on the most vulnerable areas under the incoming CC hazards. For this purpose, a detailed step-by-step guide, based on open access data, is provided and explained, ensuring that the standardization of the research makes it replicable. Such contribution is important for urban thermal environment assessment, especially during prolonged heat waves. The diagnostic character makes it useful to policymakers to prioritize necessary interventions.

2. Materials and Methods

This study proposes a three-step methodology, based on the following: (a) open access remote sensing data; (b) GIS processing and analysis; and (c) qualitative and qualitative hotspots assessment, a step-by-step guide. All the research is based on open access data freely available (Table 1). The heat-related parameters were captured on the same analysis day, while other information, such as buildings and land use, which depend on the latest updates from official sources, come from different dates. However, for the detailed analyzed zones, all the urban layers have been visually checked and contrasted with recent satellite images to avoid inconsistencies with reality. Finally, the method is tested using a real case study selected in Seville, Spain.

Table 1. Research data sources.

Data	Description	Date	Source
Local climate	Open access data of typical climate and official climate records for the studied frame	2023 29 August 2023	OneBuilding.org (epw) [62] Local weather station [63]
Land cover	Open access vectorial Land cover maps to determine the type and use of urban fabric	2018 (Last actl.)	Copernicus' CORINE programme [37]
Urban LST	Open access thermal image. Original SR of 100 × 100 m, provided resampled at 30 × 30 m	29 August 2023	USGS's Landsat 9 [24,64]
Buildings data	Open access cadastral GIS layers of built environment with age, area and height data	2022	Cadastre [65]
LCZ	Classification according to the original source guidelines	Ago-2023	Stewart and Oke [27]
Tree plans	Open access GIS layers with position, species and size of urban trees, or true colour satellite image	Ago-2023	Local databases, alternatively, NDVI
NDVI	Processed image from an open-access satellite image band	29 August 2023	USGS's Landsat 9 [24] or EOS's CropMonitor [66]

2.1. Remote Sensing Predictive Model

This methodology workflow and the guidelines are summarized in Figure 1. As this work presents a methodology that can be replicated in other case studies, it is initially presented in a generic and detailed manner, avoiding any case data. Subsequently, a specific and representative case study, the city of Seville, is selected, providing all the necessary data. The methodology is then applied to evaluate its potential in obtaining results and discussing them.

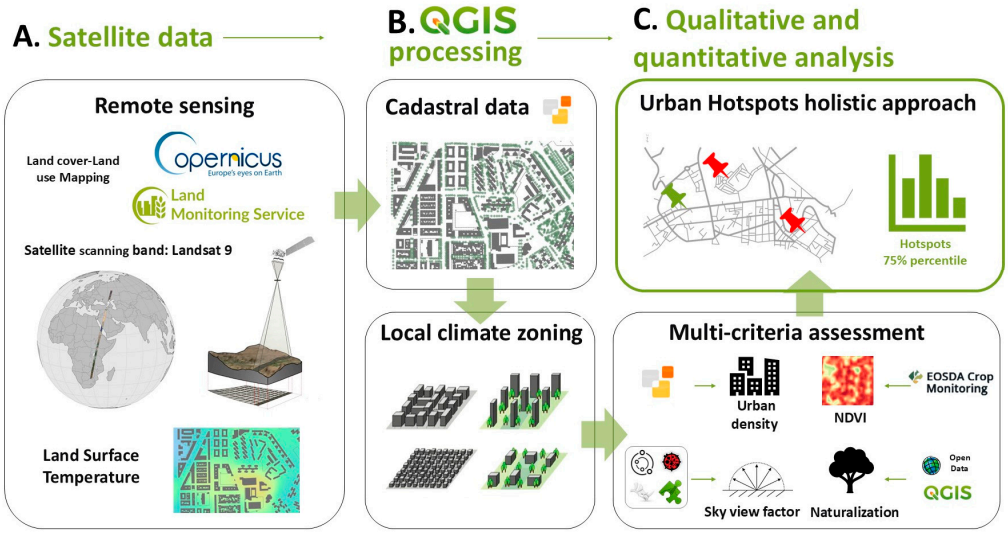


Figure 1. Graphical representation of the methodology workflow with identification of the applied tools and processes.

2.1.1. Area of Study and Time Frame Selection

The initial phase of the methodology involves the identification of the urban case study and the definition of the time frame for analysis. As outlined below, this methodology is specifically tailored to urban environments, with a particular emphasis on warm cities. Within the selected location, the climatic characteristics of the city must be meticulously detailed and analyzed beforehand. The climatic classification is determined using the internationally recognized *Köppen* system [67], while specific climatic parameters are obtained from authoritative official records. A thorough understanding of the location,

including its climatic type and prevailing local weather conditions, is essential for selecting an appropriate time frame.

Considering that the study focuses on thermal hotspots, it is preferable to select a warm day for analysis. This day must accurately represent the city's typical thermal conditions during its warm season. If this is not possible or is needed to base the study on different climatic conditions, it is possible to repeat it for several days. To ensure this representativeness, a comparative analysis between the city's climatic norms during summer and the selected day's meteorological conditions is required. Thus, to ensure the validity of the analysis, it is crucial to confirm that the selected day is clear, with no high levels of pollution or dust in the air. Additionally, the climatic variables of the chosen day, such as air temperature and radiation, should be representative of the warm season. It is also important that the wind speed on the selected day is low and below the annual average to avoid the alteration of the effects of the urban heat island [68].

Additionally, the chosen day must align with the satellite data acquisition schedule, ensuring that typical warm weather coincides with the satellite observation. The acquisition schedules for various satellite missions, including the Landsat 9 used by this research [64], are publicly accessible online.

2.1.2. Land Use–Land Cover

The initial step involves obtaining the LULC layer information for the city from the open-access CORINE programme database [37]. The most recent update from 2018, (it needs to be revised with actualized images in rapidly changing urban areas) provides a GIS vector layer with standardized LULC data featuring a geometric resolution accuracy of <10 m [37]. This dataset offers critical insights into the types of land portions within each zone, which are strongly correlated with radiation exposure and typical thermal behaviour. Furthermore, the map identifies residential areas, which are utilized for cropping and focusing on subsequent stages of the study. The use of this classification allows, on one hand, the subdivision of the city into globally recognized land zones, and on the other, the identification of urban evolution patterns. It facilitates easy comparison of this city with others and provides a preliminary estimate of the expected thermal behaviour based on land use types and typical materials, all with a high spatial resolution of 10 m appropriate to urban micro-scale studies.

2.1.3. City's Land Surface Temperature

Once the urban case study and date have been determined, and the land cover information contextualized, the focus shifts to analyzing the LST at a micro-urban scale. Diurnal LST images of the urban surface layer are obtained from the Landsat 9 satellite [16]. These images are freely accessible on the Earth Explorer platform provided by the USGS [69], where thermal band L10 data are made available. Landsat 9 introduces the novel Level 2 processing product, which provides spectral and atmospheric corrections across various bands. As reported in the literature and by the data provider [70], the LST can be derived with high accuracy (ranging from 0.4 to 1.98 K) using minimal post-processing via the QGIS raster calculator.

The Band 10-LST image can be downloaded in GeoTIFF format. Although the original data acquisition SR of B-10 is 100 × 100 m, USGS provides it with a resampled SR of 30 × 30 m, making it equal to the Landsat 9 non-thermal bands. This raster file is subsequently uploaded into QGIS, where urban map layers, sourced from authoritative bases such as cadastral websites [65] and global open-access repositories [71], are already integrated. Subsequently, the SR of the thermal image is enhanced to improve the visual interpretation of thermal distribution at the micro-urban scale. To that end, and

through geoprocessing in QGIS, the image resolution is refined to 5 × 5 m using a bicubic 4 × 4 Kernel interpolation. This process analyses the 16 nearest pixels to perform resampling, thus improving visualization quality. Bicubic interpolation is widely adopted in image processing for enhancing image clarity [72] and supporting reclassification tasks [73]. The algorithmic basis of Kernel involves this bicubic interpolation method, which is chosen for its ability to maintain the integrity of the original data while enhancing resolution [72]. This method ensures accuracy by carefully considering the values of the surrounding pixels, thus avoiding the introduction of artifacts. Additionally, the interpolation process is designed to prevent over-smoothing, which can obscure important thermal details. Maintaining the original temperature thresholds ensures that the refined images are both accurate and reliable while enabling efficient computational processing within QGIS.

Once the rescaled image is obtained, it is delimited and cropped according to the administrative boundaries of the city and overlapped with urban layers and building footprints. The analysis then specifically targets the LST of streets and urban open spaces located between built structures.

2.1.4. Residential Area Delimitation and LCZ Classification

The study prioritizes homogeneous residential settlements, with particular attention to urban public livable spaces such as streets, squares, and unbuilt areas. To this end, it is necessary to delineate the AOI to focus exclusively on residential-use zones. Industrial and infrastructure areas, which typically exhibit significantly higher diurnal LST values, as well as parks and large green spaces with lower LST values, are excluded as they do not accurately represent thermal patterns in residential streets and public urban spaces [74]. To define this AOI, the CORINE LULC [37] map is utilized to identify and crop residential-use areas, which are then overlaid with the thermal LST map. The LST thresholds for the selected AOI are reassigned according to the new LST boundaries. The resulting AOI is then classified into LCZ categories [27]. This cross-evaluation of surface temperature and LCZ is not novel in the literature, but as in previous studies [28–30], it helps to divide the urban fabric into homogeneous zones, which, according to the literature, tend to have similar thermal behaviours. Additionally, a complementary analysis is proposed where urban and thermal aspects are combined with an evaluation of vegetation and the resulting SVF. This strengthens the results and comparisons between zones and confirms the hypotheses put forward by the authors of the original LCZ study [27].

While automated LCZ classification methods are widely acknowledged in the literature [58,75], they often face challenges in achieving the resolution necessary for micro-urban scale analyses, particularly due to their dependency on the availability and quality of training areas. As highlighted by [76], automated methods are effective for large-scale analyses but may lack the specificity required to accurately represent local urban features, as can be seen in many available maps [77]. On the contrary, LCZ classification, based on site data, visual interpretation, and expert knowledge, accurately matches the local features [27,78], but can also become labour-intensive. This study adopts a hybrid GIS-based approach, combining detailed GIS parameters, expert knowledge, and satellite imagery validation. The classification process was curated in QGIS and supervised by the authors' knowledge of regional urban morphology. This hybrid methodology leverages the advantages to ensure a reliable classification tailored to the specific case study characteristics. Although it can become more time-consuming, this approach is particularly suitable for single-city case studies where capturing micro and local specificity is critical. For broader-scale studies, however, remote sensing and automated methods provide a more efficient and reproducible alternative, as noted by [76].

2.1.5. Hotspots' Detection and Multi-Criteria Assessment

Once the extracted residential area LST raster overlaps with the LCZ classification, the hotspot detection is addressed. This study proposes a two-phase detection of thermal hotspots, based on the distribution of temperatures and the concentration and density of hot zones. Initially, the analysis begins with the distribution of temperatures within the threshold, identifying extreme values and their distribution. Subsequently, the temperature quartiles of the AOI are calculated, establishing the temperature value equivalent to the third quartile as particularly warm, as previously used in the literature [56]. Thus, the first phase isolates the areas with the top 25% of temperatures. Following this, using QGIS software tools, a proximity and density cluster analysis is conducted to obtain truly representative hotspots and ignore irrelevant ones. With the selected hot pixels and a transformation to vectors, a clustering process is performed based on the original data grid, in this case, a 100 × 100 m SR from Landsat 9. Clusters of pixels containing particularly warm temperatures and grouped in sets larger than one original pixel are considered. After this phase, the hot and relevant clusters in proximity and density have been selected, disregarding isolated and non-representative areas. In this way, the hotspots of the AOI have been obtained and can be represented on the map.

After that, with all thermal hotspots represented in the city, this research proposes the selection of two specific hotspot areas based on their urban uniformity. These two hotspot areas are compared with two other areas that exhibit lower temperatures. The main urban heat-related parameters of the final four selected areas are extracted and assessed to determine their influence on urban overheating. The methodology proposed allows a discussion based on the cross-analysis of these parameters results. They are calculated from open access and official sources data, in the first term they are obtained graphically, in the form of maps or heatmaps. Then, the main statistics are extracted in summarized tables, and finally, the values distribution graphs are obtained. In this way, a complete cross-evaluation can be made.

- Building environment and pavements

The building layers are obtained from cadastral sources [65], which in many countries include information on the geometry, area, height, and even age of buildings. The pavement layer can be obtained from municipality open data. Four different parameters are studied, all using the official GIS layer information.

- Building surface fraction (BSF): a ratio that expresses the percentage of the total AOI surface that is occupied by the floor area of buildings.
- Floor area ratio (FAR): buildings' gross floor area to the size of the lot upon which they are built.
- Mean building height (MBH): the weighted average height of all buildings in the AOI.
- Pavement permeability fraction: ratio of pervious pavement to the total AOI paved area.

- Land surface temperature

The LST of the studied area is analyzed on the unbuilt area. This is shown as a heatmap, and the main statistical values are extracted from the images using the QGIS raster analysis tools. The mean, maximum, and minimum LST are obtained, subsequently, the values' distribution per pixel is analyzed.

- Green structures

Two measurements are assessed as they have an important impact on sun radiation and LST.

- Tree canopy fraction: ratio of tree-covered area to the total AOI area. Data are obtained from official local administration sources. However, it can also be supported by LIDAR maps.
- NDVI: studies the quantity and health of the vegetation. Although it can be obtained directly from satellite images (Landsat 8–9 or Sentinel 2), in this case, Crop Monitoring [66], was used.

The results are shown, firstly, as a 5 × 5 m SR heatmap superimposed on the city's urban layers. Secondly, its main statistical values—mean and maximum NDVI are obtained from the raster (minimum is always 0 in cities, as it represents areas with no vegetation, negative values that are used to represent water, snow or clouds could not be present in the AOI).

- SVF

SVF was calculated based on a 3D model imported from QGIS urban layers using Rhinoceros-7 3D CAD software. Graphic programming plugins Grasshopper, Urbano 1.4.2 [79] and Ladybug 1.7.0 [80] were then used. This paper has the novelty of considering the trees and the space under them in the consideration of the SVF, as most of the study only considers the building context, or considers the SVF on the top of trees, which is inaccurate. Thus, SVF is calculated based on the main urban environment (3D buildings and trees), according to previous studies [40]. A 5 × 5 m SR is set for the pixels grid of the resulting image, as the LST raster. The SVF heatmap is uploaded to QGIS and overlaps on the urban layers. Finally, the main statistical parameters, mean and maximum SVF, are obtained for each AOI.

2.2. Field of Application

The field of application for this research is urban settlements in warm regions. Given that the aim is to identify hotspots and analyze the causes and consequences of hot climates in urban spaces, the study focuses on cities located in temperate and hot climate zones. Furthermore, as the study is based on open GIS data, available geospatial data are necessary to develop the methodology properly.

2.3. Case Study for Methodology Application

In order to apply the methodology presented and to test the possibilities in a real scenario, the case study selected is the city of Seville in the southern Spanish region of Andalusia, one of the warmest regions in Europe (Figure 2). Seville is the most populated urban settlement in the region, with 684,000 inhabitants (last census 2022) in the municipality. Therefore, it is catalogued as a metropolitan area according to the OECD classification [81]. The city has a *Csa Köppen* climate [67,82], characterized by hot and dry summers, warm midseason, and temperate winters. Seville can be considered a representative example of a medium-large cities in the Mediterranean area. It is a significant urban settlement subjected to a warm climate, featuring a historically dense centre and several recently developed outer areas with diverse urban typologies. Therefore, its location, urban characteristics and distribution, population, and climate make it a proper example of southern European cities. The results and conclusions derived from this study could be extrapolated and compared with those from other similar cases. Appendix A.1, at the end of the document, shows specific data and climate registers for Seville for a full year.

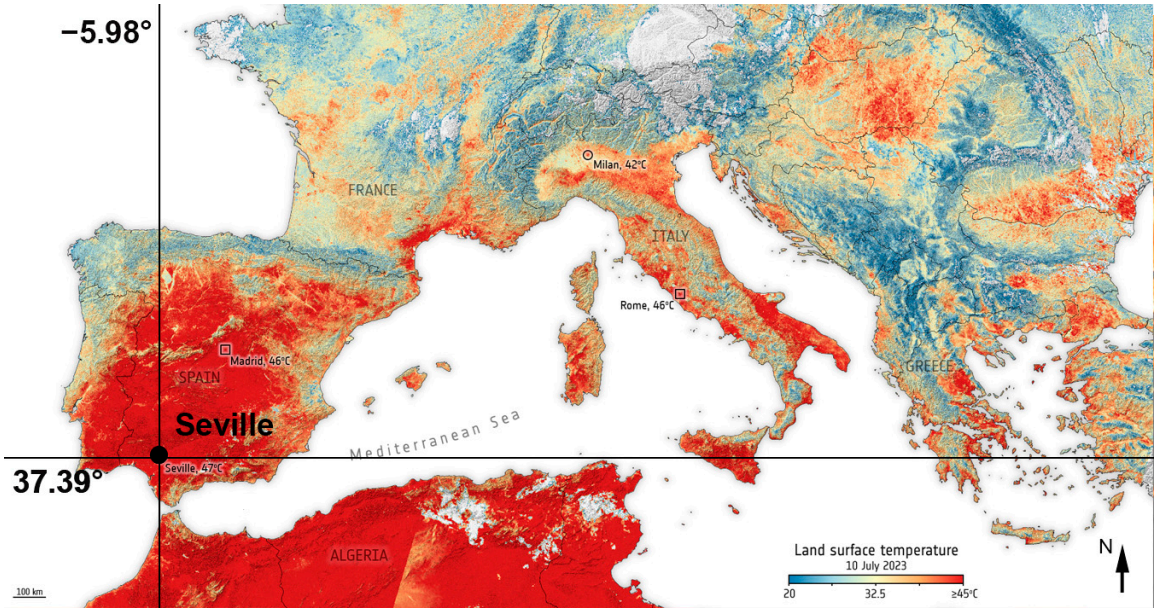


Figure 2. Case study location. Southern Europe LST during a heatwave in the summer of 2023 (10 July 2023). (Source: reprinted/adapted under license CC BY-SA 3.0 IGO from ESA. [83], 2023).

3. Results and Discussion

This section shows the results of the methodology detailed in Section 2, now applied to the city of Seville, as a pilot case study, in order to test the operation of this urban assessment method. In parallel, the results are also discussed in each subsection with diverse focuses, all supported by the figures.

3.1. Area of Study and Time Frame Selection for the Case Study

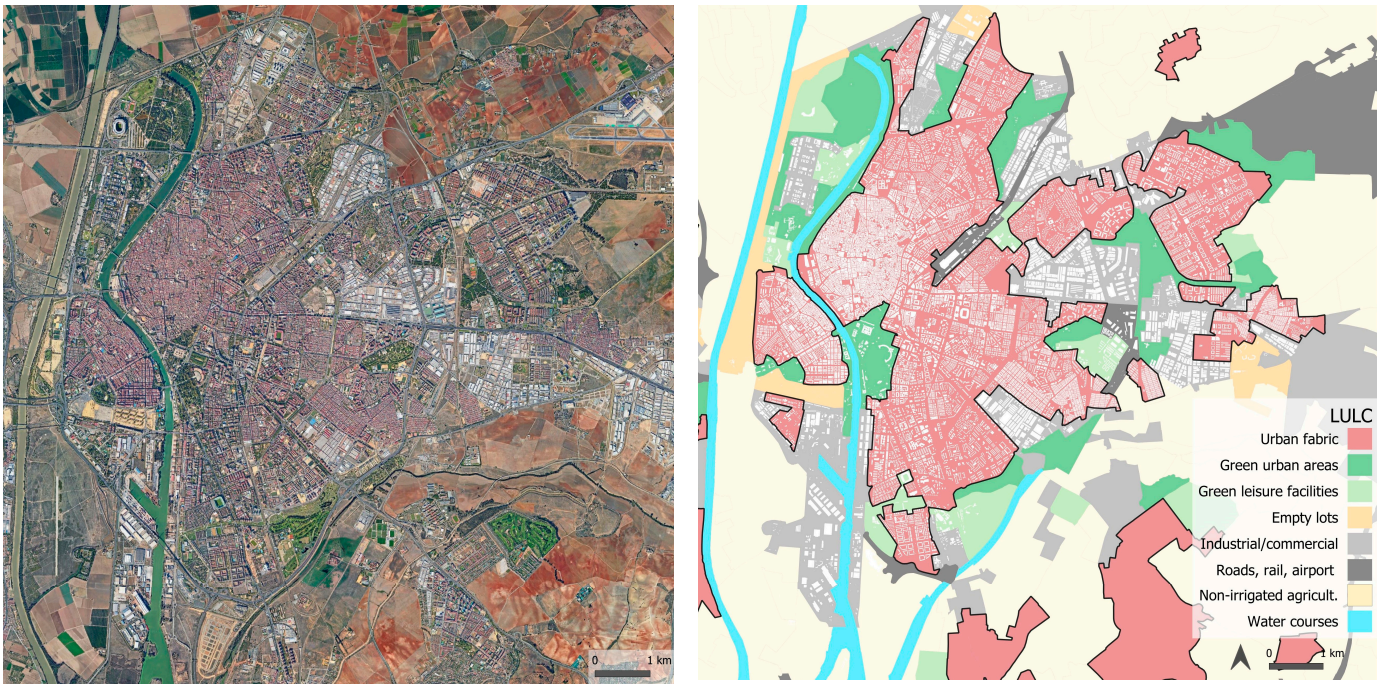
The selected day is 29 August 2023. This day Seville experienced a warm day, typical of the season. Besides the satellite acquisition, the climatic conditions during the day were representative of the warm season. Appendix A.2 provides detailed climate data for this specific day. The recorded data are compared with the average values for a typical day in the warm season in Seville (15 June to 15 September), showing a good match:

- Clear day without relevant episodes of pollution or atmospheric dust;
- Mean air temperature: 29 August: 30.3 °C _ Warm season: 30.0 °C;
- Mean global radiation: 29 August: 270 W/m^2 _ Warm season: 295 W/m^2;
- Wind speed: 29 August: 2.07 m/s _ Warm season: 2.78 m/s.

It should also be noted that there were severe drought conditions in the region in the selected period; therefore, most of the grass and wild low vegetation was dry due to the summer heat and water lack, which affects the effective low vegetation surface temperature.

3.2. Land Use–Land Cover Results

A first context of the city is provided, as well as the LULC map, which allows one to distinguish between diverse urban uses and land types. This is obtained from the Copernicus' CORINE maps [37]. The layer is then processed in QGIS with only minimal corrections. The resulting map is shown in Figure 3.



(**a**) (**b**)

Figure 3. (**a**): Real colour satellite image of Seville, ©2023 Google [84]. (**b**): LULC image of the city [37].

3.3. City's Land Surface Temperature Results

The LST for Seville was taken by Landsat 9 on 29 August 2023 at 11:00 (original Band 10 file called: LC09_L2SP_202034_20230829_20230831_02_T1_ST_B10). Through the application of the exposed methodology, the LST for public spaces is obtained. The resulting image (Figure 4) shows the LST of the non-built areas, that is, the open urban spaces of the city with a very high resolution of 5 × 5 m, thanks to the Kernel spatial interpolation previously exposed in the methodology. As the temperature range for the whole city LST is 30–55 °C, at a specific point in time, a difference of 25 °C can be observed within the city.

Discussing first the whole city case study scale, and according to Figure 3b (LULC) and Figure 4 (LST), what first becomes apparent is the strong relationship between the kind of land cover and its LST. This was already pointed out by previous research [36]. These classes tend to exhibit more uniform climatic behaviour within the city due to the commonly present materials and their properties concerning heat fluxes (albedo and emissivity), heat capacity (thermal mass), as well as the typical presence of vegetation and urban density (SVF), among others. Furthermore, the LULC classification facilitates a targeted focus on the residential compact fabric, which is the primary subject of this research.

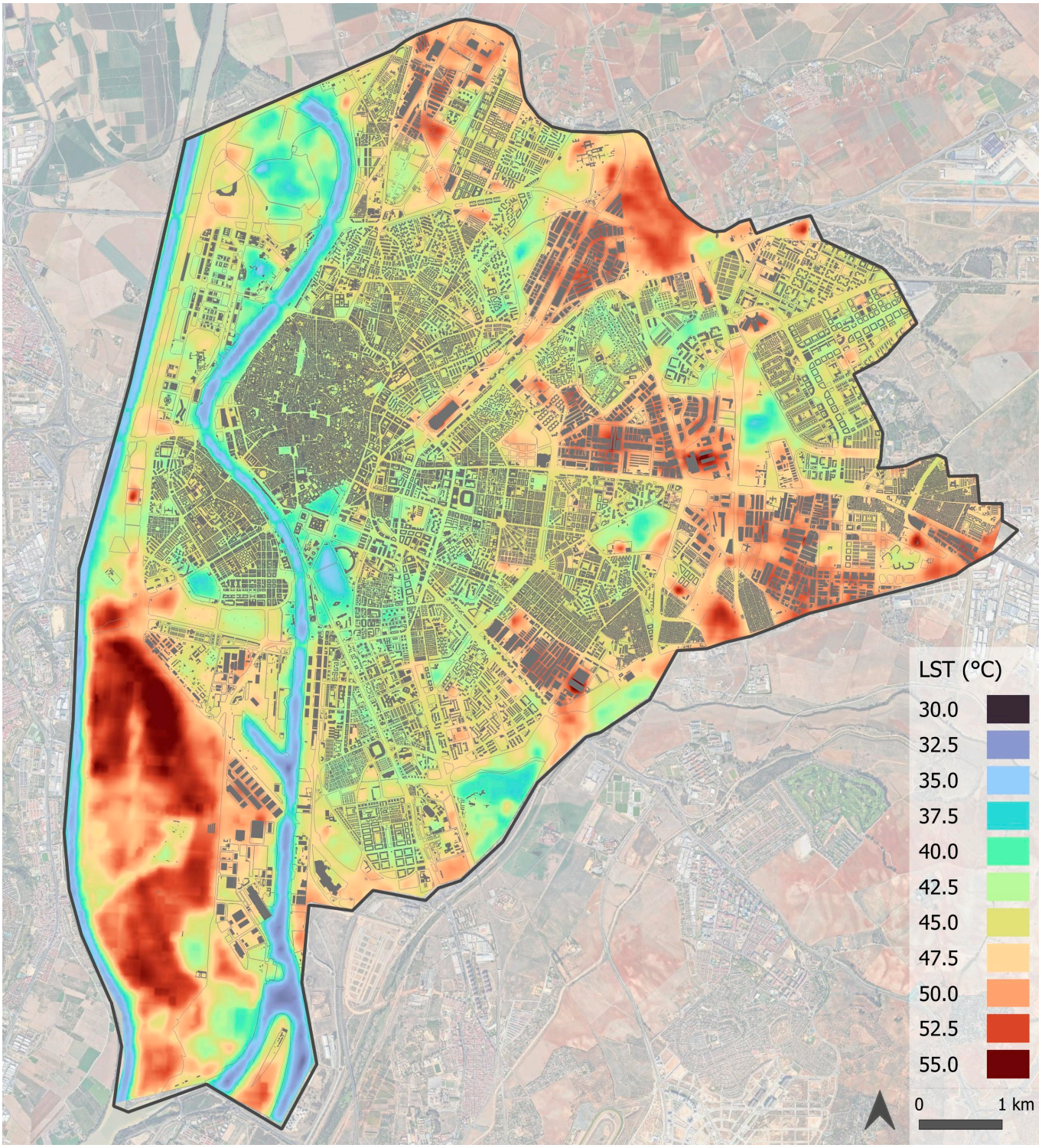


Figure 4. LST recorded by Landsat 9 satellite in Seville on 29 August 2023, at 11.

Now, thanks to the very high-resolution maps, it is possible to analyze the heat performance at the micro-urban scale, which is a novelty compared with other approaches [20,50,59,60], allowing for a more accurate assessment. The LULC and LST comparisons evidence how the non-urban areas of dry fields, which are totally exposed, are the warmest. This demonstrates that in temperate zones, non-irrigated low vegetation not only fails to reduce temperature but can actually worsen thermal comfort. In addition, industrial and infrastructure areas constitute warmer zones due to their typical materials

and large exposed metal roofs. Although this is caused by their characteristics and urban configuration, it should be noted that this warm effect could also extend to nearby areas, affecting the microclimate of the surroundings. This proves the great importance of selecting urban materials, as seen in this and previous research [45,85,86], as they have the capacity to strongly influence and change the near urban climate, and thus the thermal perception of the inhabitants.

In contrast, Figure 4 shows several cooler areas that stand out in the city. The most notable is the river, where the water surface is almost 25 °C lower than the hottest surfaces in the city, but also the big green parks, where a decrease of 20 °C can be noted. In the case of the former, the low temperatures are due to the high thermal inertia of the water, which retains the cool night-time temperatures, although this inertia can have the opposite effect during the first few hours of the night. In the case of parks, this image shows the capacity of the big green mass to reduce temperature due to the evapotranspiration and regulatory processes of foliage, as proved by other studies [87]. However, dry fields prove how vegetation with no water access or exposure to high temperatures can produce detrimental effects. On a city-wide scale, the affection of these cooling points is important because urban areas surrounded by cooler zones will experience more temperate conditions and can improve comfort levels. Finally, the compact urban fabric (according to Figure 3b), mostly residential areas, seems to have more homogeneous temperatures, only showing slight variations in Figure 4.

3.4. Residential Area Delimitation and LCZ Classification Results

As already shown, the LST extreme values are observed in non-residential areas, while the residential does seem to exhibit slightly homogenous temperatures. Therefore, this research focuses on the residential areas. According to Section 2.1.4, they must be cropped using the CORINE land cover delimitation (Figure 3). Thus, LST focus is delimited on the residential areas, which resulting map is shown in Figure 5. This area is classified according to LCZ classification [27], as indicated in Section 2.1.4. Four LCZs are identified:

- LCZ 2: Compact midrise;
- LCZ 3: Compact low-rise;
- LCZ 5: Open midrise;
- LCZ 6: Open low-rise.

The residential LCZ areas are overlapped on the new cropped LST heatmap and a new residential LST range of 40–50 °C is found. Thus, although previously it seemed to be homogeneous, differences of up to 10 °C LST between different residential urban areas are now found and represented (Figure 5). Moreover, individual LST maps according to the LCZ categories are shown in Figure 6 so that they can be analyzed and discussed separately. At the same time, extension and LST data are summarized in Table 2.

Table 2. Residencial LCZ data for the city of Seville (SVQ).

Zone/LCZ	Surf. (ha)	%	LST (°C)		
			Mean	Max.	Min.
SVQ	8088.8	-			
SVQ Resident. Area only	3097.7	38.3			
LCZ 2	369.4	11.9	43.7	47.8	37.8
LCZ 3	1043.1	33.7	44.9	50.6	37.8
LCZ 5	1482.4	47.9	44.6	51.0	40.2
LCZ 6	202.8	6.5	43.6	49.0	40.8

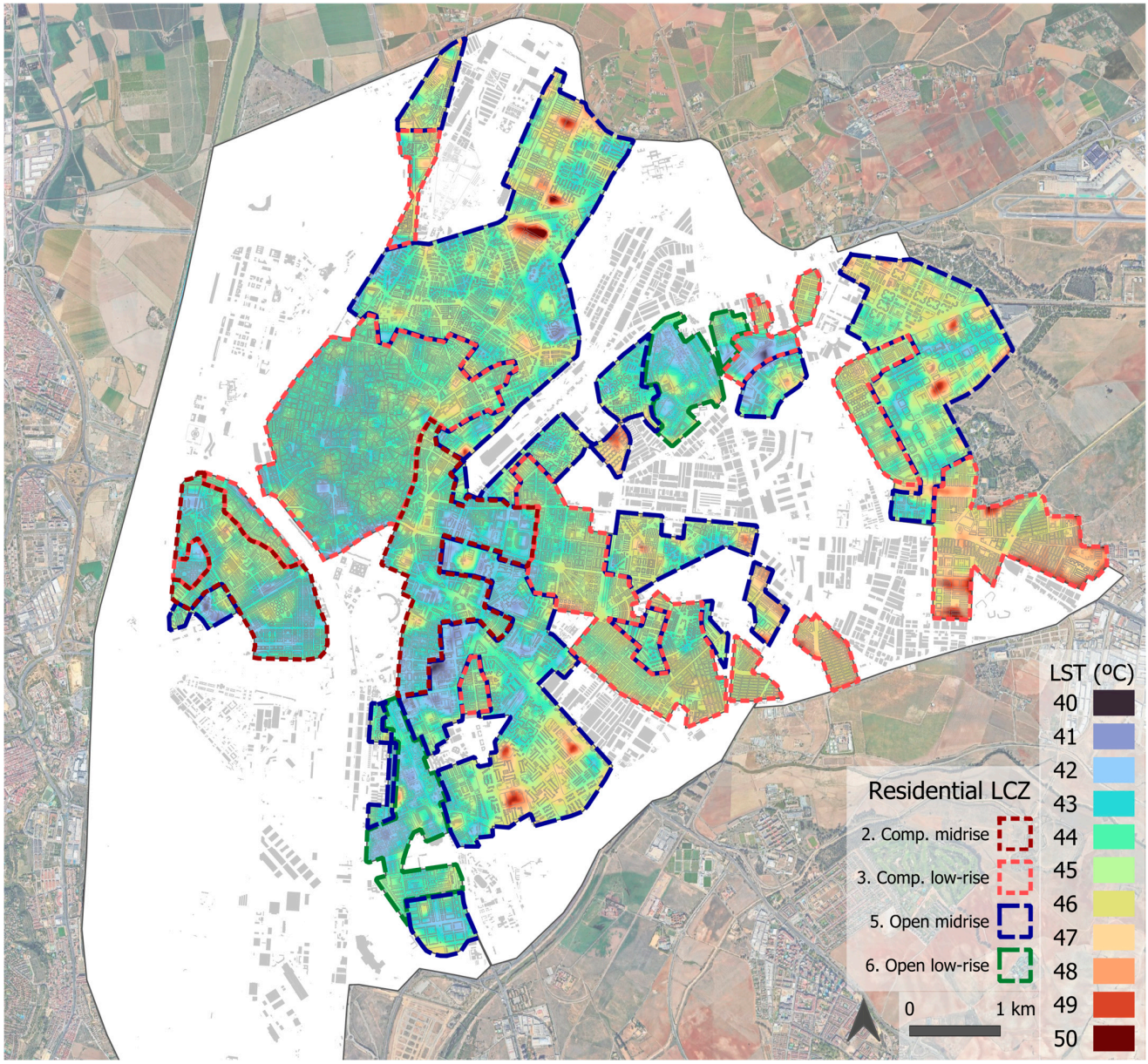


Figure 5. The residential area of Seville, LCZ classification and LST recorded by Landsat 9 satellite in Seville on 29 August 2023, at 11.

The first notable aspect is the irregular presence of different LCZs in this city, with a high prevalence of LCZ 5 (48% of total residential area) while LCZ 6 is the least abundant, accounting for only 6.5% of the total, as shown in Table 2. Focusing on Figure 6 and based on the LST of each zone, there are some aspects to be noted. Some degree of LST uniformity can be observed in LCZ 2 (Figure 6a) and LCZ 3 (Figure 6b) in the city centre area, both zones with highly compact and homogeneous urban fabrics. Moreover, both LCZ 2 (Figure 6a) and LCZ 6 (Figure 6d) display the lowest LST in the city according to the mean and extreme temperatures (Table 2). In contrast, LCZ 3 (Figure 6b) and LCZ 5 (Figure 6c) both show heterogeneous but higher LST. According to the obtained results, the uneven presence of various LCZs becomes increasingly important as they are strongly linked with the tendency to suffer higher temperatures. In the case of Seville, and according to Table 2 and Figure 6, the residential fabrics that are more prone to experiencing high temperatures due to their urban characteristics are the LCZ 3 and LCZ 5, and they represent 81.6% of the total residential area of the city.

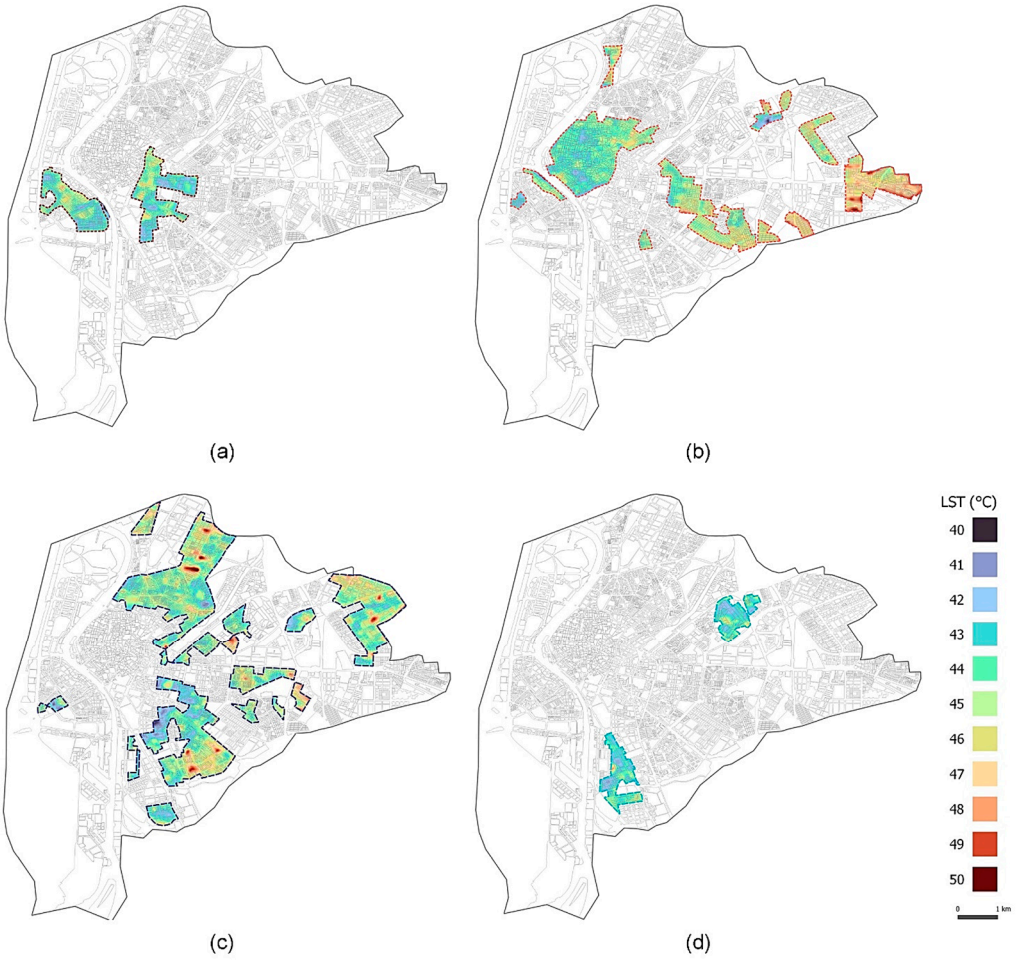


Figure 6. Residential LCZ of Seville. (**a**) LCZ 2: Compact midrise. (**b**) LCZ 3: Compact low-rise. (**c**) LCZ 5: Open midrise. (**d**) LCZ 6: Open low-rise.

3.5. Hotspots' Detection and Multi-Criteria Assessment Results

Several warm areas can be easily observed in Figures 5 and 6; however, the thermal hotspots are now statistically located and clustered according to Section 2.1.5. Thus, the pixels above the 75th percentile of heat (the 25% warmest of the total residential areas), grouped according to density and proximity, are calculated and mapped in Figure 7. The first aspect that this result highlights is the fact that the calculated Seville diurnal hotspots represent almost 11.2% of the total residential area of the city.

Furthermore, some particularities can also be commented on. The performance of this reclassified image (Figure 7) further highlights the great capacity of adjacent warm areas to affect and overheat residential areas near the city boundaries. It is the effect of hot outer rural areas and industrial zones that, through the re-emitted longwave radiation and air convection, are able to heat both the area itself and the surrounding areas. These results show how residents who live in peripheral neighbourhoods or are surrounded by industrial districts are more exposed to heat than others in the inner parts of the city.

Another aspect to highlight is that the centre of some of the most intense hotspots are artificial-grass sports fields. Artificial grass areas reach significantly higher temperatures than natural green areas and maintain high temperatures for longer [86]. This phenomenon can be attributed to the high thermal inertia of the impervious concrete base, and the low albedo of the artificial grass, which results in greater heat absorption and slower cooling rates. This phenomenon illustrates how anthropogenic factors, such as recreational activities, contribute to urban heat patterns. The spatial distribution of these hotspots

underscores the need to consider specific urban features and their impact on local thermal environments. Far from being anecdotal, thanks to the resulting images, the research confirms how these local elevated LST values also influence the temperatures of the closest neighbourhoods, in line with previous research [19]. This should be taken into account in urban planning and in the design of facilities for cities, conscious of the consequences that the selection of specific materials and systems has for the closest urban climate.

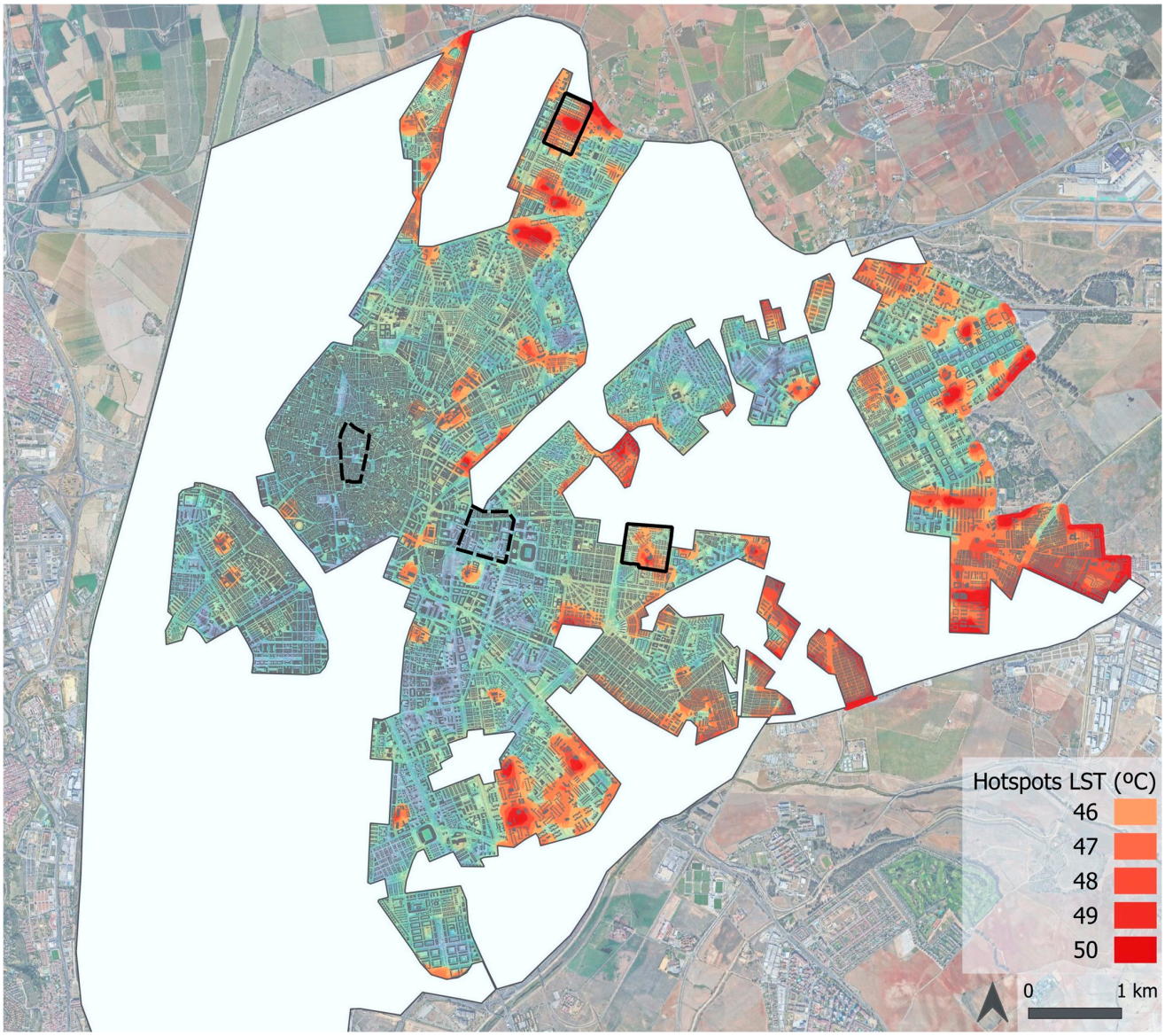


Figure 7. Seville residential area's thermal hotspots (Reds). The continuous polygons represent the selected hotspots, while discontinuous polygons represent the selected temperate zones, all chosen for further analysis.

When analyzing the city hotspot distribution, and supported by the previous classification images, it was obtained that most of the thermal hotspots are concentrated in LCZ-5 areas, so these zones seem to be more prone to diurnal overheating. These areas are typically located in peripheral neighbourhoods, most of which were developed during the mid-20th century [88] as new residential developments. They have urban features that are common in many European cities, making these results more relevant and applicable to other case studies. The overheating of these LCZ-5 classified neighbourhoods can be explained by several factors. Firstly, they are typically located on the outskirts of

the city, surrounded by hot areas such as crop fields, industry, or infrastructure. Within these neighbourhoods, a key factor is the urban planning employed. These areas were designed with significant spacing between buildings, meaning high SVF, and therefore, greater exposure to solar radiation, as previously noted [27]. Additionally, these wide and open public spaces usually lack substantial green masses, resulting in low NDVI values, which translates to a lack of shade and green cooling. Finally, these areas are often characterized using heavy materials such as concrete, cement, and asphalt parking lots, all with medium to low albedo and high thermal inertia, ensuring overheating and subsequent slow cooling through the progressive emission of longwave radiation into the urban space. This analysis highlights the influence of both urban planning and anthropogenic factors on urban thermal configuration, underscoring the need for a deeper consideration of these aspects.

It is necessary to highlight that this type of urban zone, LCZ-5, is the most prevalent in the city of Seville, accounting for 48% of the total residential surface area (Table 2), but is also widespread across all European cities [45]. Thus, this issue fact should concern urban planners.

The results already obtained provide significant information on urban heat distribution and allow the identification of areas of opportunity for further analysis or intervention. However, this research also proposes a more in-depth analysis approach of selected zones, studying the main parameters relating to urban heat. Therefore, to test the possibilities of this cross-assessed method, two hotspots are compared within other two temperate areas, considered as control zones (Figure 7). This enables the comparison of their individual heat-related parameter values, discussing the causes of the differences in the LST and the reasons why some become hotspots while others do not. The urban contexts of the selected zones and the final selected cropped areas are shown in Figure 8.

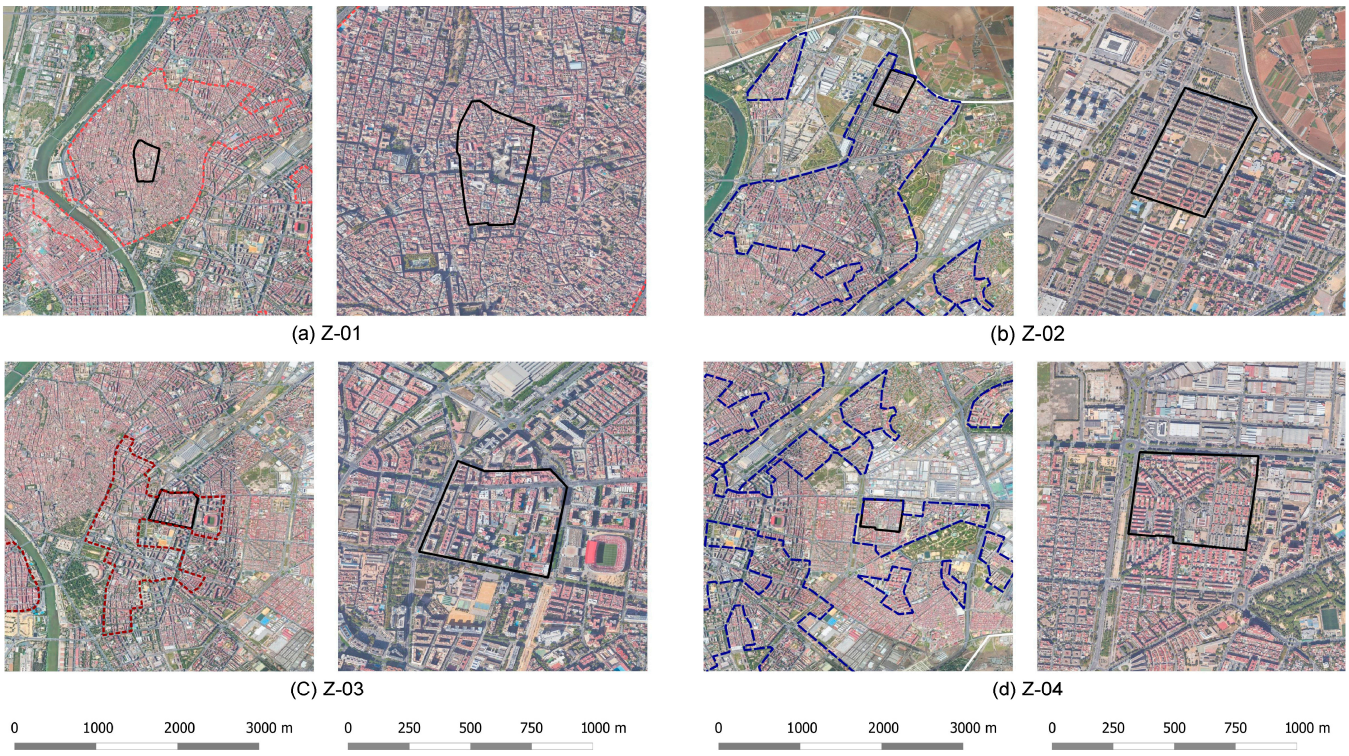


Figure 8. Urban context and location of the selected assessed zones: Temperate control areas: Z-01 (**a**) and Z-03 (**c**). Hotspots: Z-02 (**b**) and Z-04 (**d**).

The following sections show the results of the urban parameters obtained according to the methodology previously detailed (Section 2.1.5), for the selected zones. The results of these parameters are shown in the form of maps (Figure 9), while the main data are calculated in Table 3. Classification of selected areas according to LCZ types:

- Z-01: Temperate area. Historic city centre zone, LCZ-3;
- Z-02: Hotspots. Northern neighbourhood zone, LCZ-5;
- Z-03: Temperate area. Modern city centre zone, LCZ-2;
- Z-04: Hotspot. Eastern neighbourhood zone, LCZ-5.

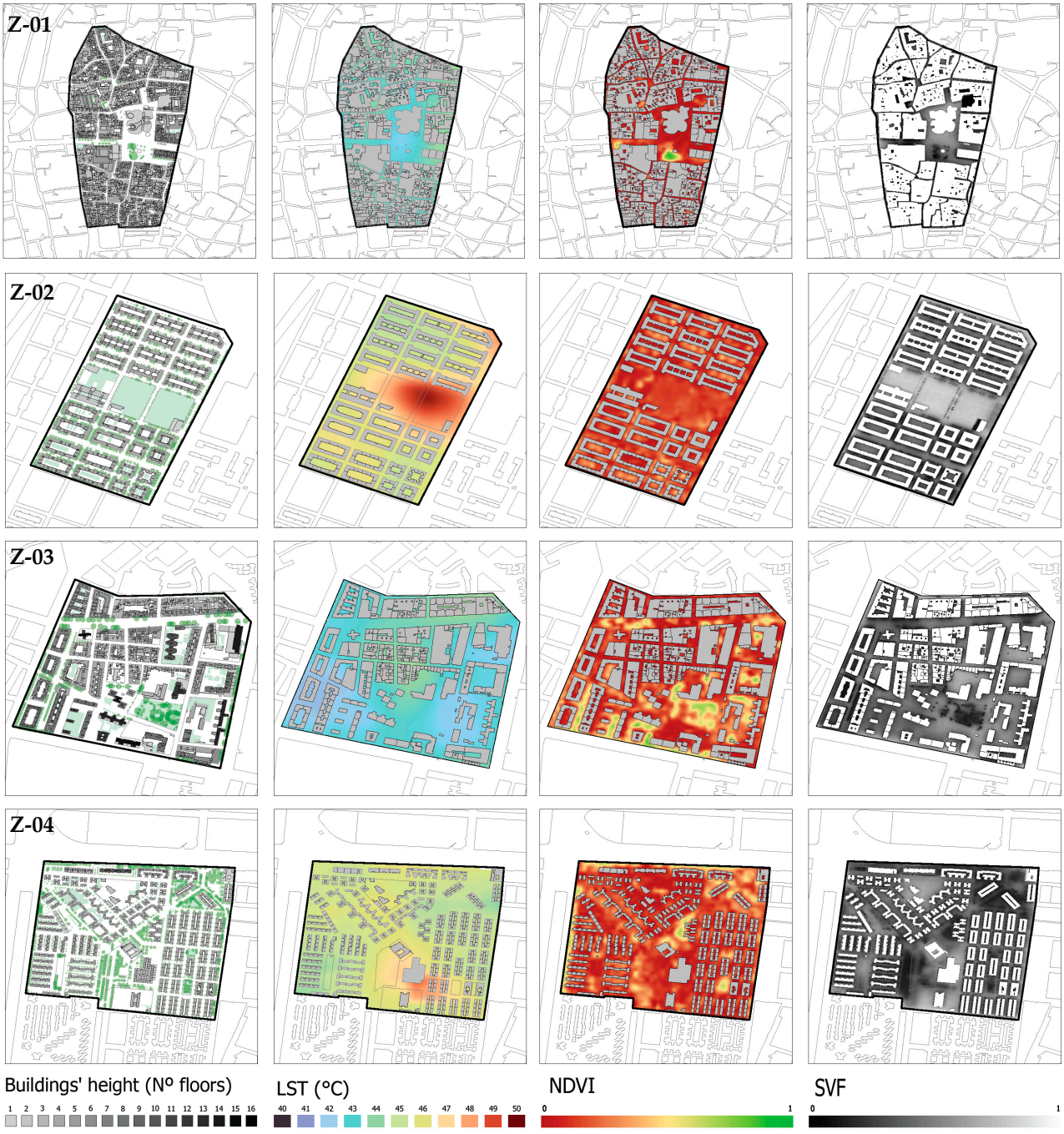


Figure 9. Graphical display of the analyzed urban parameters. From the top: Z-01, Z-02, Z-03, and Z-04.

Table 3. Urban data results.

Zone	LCZ	Build. Env. & Pavemt.				Land Surf. Temperature			Green Structures			Sky View Factor	
		BSF (%)	FAR	MBH (m)	Perv. Surf. (%)	Mean (°C)	Max. (°C)	Min. (°C)	Tree Cnp. (%)	NDVI Mean	NDVI Max.	Mean	Max.
Z-01	LCZ-3	70.3%	2.3	9.8	0.1%	43.4	44.5	42.3	1.3%	0.09	0.88	0.34	0.82
Z-02	LCZ-5	32.5%	1.2	11.2	14.4%	46.4	49.7	44.7	9.3%	0.14	0.46	0.43	0.84
Z-03	LCZ-2	42.0%	2.0	14.7	8.5%	43.0	44.5	41.6	5.3%	0.22	0.81	0.38	0.81
Z-04	LCZ-5	25.2%	1.0	12.0	4.6%	45.6	48.6	44.2	13.3%	0.17	0.72	0.29	0.82

3.5.1. Building Environment and Pavements

The first column in Figure 9 shows the graphical analysis of the built and paved urban GIS layer information.

- Building surface fraction (BSF): The large differences in the percentage of areas occupied by buildings can easily be seen on the maps, as reflected in the results (Table 3). The BSF percentage of Z-01, 70.3%, should be noted, as it corresponds to an extensive and dense historic city centre, while the typical range given in the literature for this LCZ is 40–70% [27]. This is followed by Z-03, with 42.0%, a low value, despite the LCZ source classification as dense fabric. The percentages for the other two zones—Z-02 and Z-04, hotspots, and open urban fabric areas, stand at 32.5% and 25.2%, respectively, while the given range for these types of fabric is 20–40%.
- Floor area ratio (FAR): Building height appears shaded in greyscale in the first column of Figure 9, while Table 3 shows the resulting ratio between the total built area and the total extension of the zone. Z-01 also has the highest FAR value as it is the most densely built zone, although it is lower in height than other zones. In contrast, Z-04 is the least dense zone and has the lowest floor area ratio.
- Mean building height (MBH): The calculated data are shown in Table 3. The highest mean height is that of Z-03, 14.6 m, followed by Z-02 and Z-04, all defined as midrise LCZ, with a characteristic height of 10–25 m [27].
- Pavement permeability fraction: This is shown in the form of green paths (first column in Figure 9, while Table 3 shows the calculated data). There is a large difference between the zones, with a minimum value of 0.1% in Z-01, corresponding only to areas with trees; to the maximum value of 14.4% in Z-02, where there are several open squares full of pervious terrains.

3.5.2. Land Surface Temperature

This is the main parameter measured to determine the intensity of hotspots. The second column in Figure 9 shows the considerable differences found between the LST of the diverse zones, with differences of up to 9 °C between areas. In general, hotspot zones Z-02 and Z-04 display higher temperatures than the Z-1 and Z-3. Due to the sparser urban fabric, and thus, higher SVF, sun radiation heats the urban surfaces further, speeding up and increasing AT in the area due to the radiant heat and air convection. According to the calculated data in Table 3, the Z-02 and Z-04 mean LST are 3–4.5 °C higher than in temperate zones, while the maximum and minimum values of the hot zones are also considerably higher, with a 3–5 °C increase.

3.5.3. Green Structures

- Tree canopy fraction: An abstract representation of the tree canopy is shown in the first column in Figure 9 in the form of green circles; however, its presence and intensity are

better represented in the third column, with the NDVI graph. Green canopy calculated data are in Table 3. The lowest values are obtained by Z-01, the densest area, with 1.29% of tree cover. In contrast, the highest values are those of Z-04, the least dense area, with 13.3% of green cover.

- NDVI: Heatmaps are shown in the third column in Figure 9, where major differences can be observed, as is the case in the calculated data of Table 3. Again, the most extreme situation corresponds to Z-01, where the mean NDVI is 0.09, an extremely denaturalized value. However, this zone displays the maximum NDVI value, attributed to the presence of a large healthy tree in the middle of the central square, even though there is hardly any vegetation in the rest of the area. Moreover, it is also worth noting the high NDVI value of Z-03 which, despite having a compact fabric, has a mean NDVI slightly higher than that of other open zones, while its maximum is even higher (0.81). This is due to the presence of a small urban garden in the middle of the zone. The graphics in Figure 9 show the clear dependency between the index and the vegetation plan in the first column.

3.5.4. SVF

The sky view factor heatmaps, shown in the fourth column in Figure 9, express not only the building compactness but also the height and density of the vegetation. The results calculated are shown in Table 3. It is notable that Z-01, even with a higher built density, does not have the minimum SVF. This is due to the low height of the building and the low existence of trees that block the sky view. Moreover, the results show how even the open fabric zones, Z-02 and Z-04, have medium-low main SVF values, as the potential exposure allowed by the buildings is blocked by the existing vegetation, and so, higher NDVI. SVF, as the index that measures the sky exposure, constitutes an efficient individual measure of all the previous building density parameters, condensing all the calculations into a single value. Therefore, a considerable relation can also be observed between SVF and LST. Although there are other parameters to be taken into account, cross-referencing SVF and LST results confirms that the higher the SVF, the higher the diurnal LST.

Once the results are presented (Figure 9 and Table 3), several aspects can be discussed. Two hotspots AOI (Z-02 and Z-04) are selected together with two more temperate areas (Z-01 and Z-03), in order to obtain a cross-assessment supported by the results of the urban heat-related parameters. Moreover, a quantitative assessment has been developed in Figure 10 to support the discussion of results. Finally, it is noted that the AOIs have also been classified based on their LCZ classification, which helps the comparison between different urban fabrics and allows for extrapolations based on these standardized archetypes and expected anthropogenic performance. In this sense, the initial built environment analysis (Table 3) highlights a main aspect. The calculated values, associated with the visual LCZ classification, strongly correspond with the characteristic ranges given by the original source [27]. This confirms the effectiveness of hybrid satellite and GIS-supported classification against automatic algorithms that may be inaccurate for finer scales.

The results demonstrate the high impact that SVF has over the LST, becoming a crucial parameter to be analyzed. In fact, this method includes a novel SVF calculation at the micro-urban scale that properly considers the effect of trees, a critical urban feature not considered by some previous research [61]. This is also proved by comparing NDVI and SVF distribution (Figure 10). Moreover, the obtained results, shown in Figure 9 and mostly in Figure 10 also prove how the SVF becomes one of the principal LST-related factors. As a result, the LCZ classification of an urban area also reflects this trend, as previously shown in Figure 6. Within the analyzed AOIs, the hotspots are primarily located in LCZ-5, characterized by its sparser urban fabric, while the cooler, temperate areas are concentrated

in the denser and greener zones of LCZ-3 and LCZ-2. However, not all LCZ classes exhibit the same thermal behaviour, as highlighted in Figure 10. This variation arises from the broad nature of the LCZ classification, which encompasses diverse urban fabric types into generalized classes; however, distinct patterns emerge, offering valuable insights.

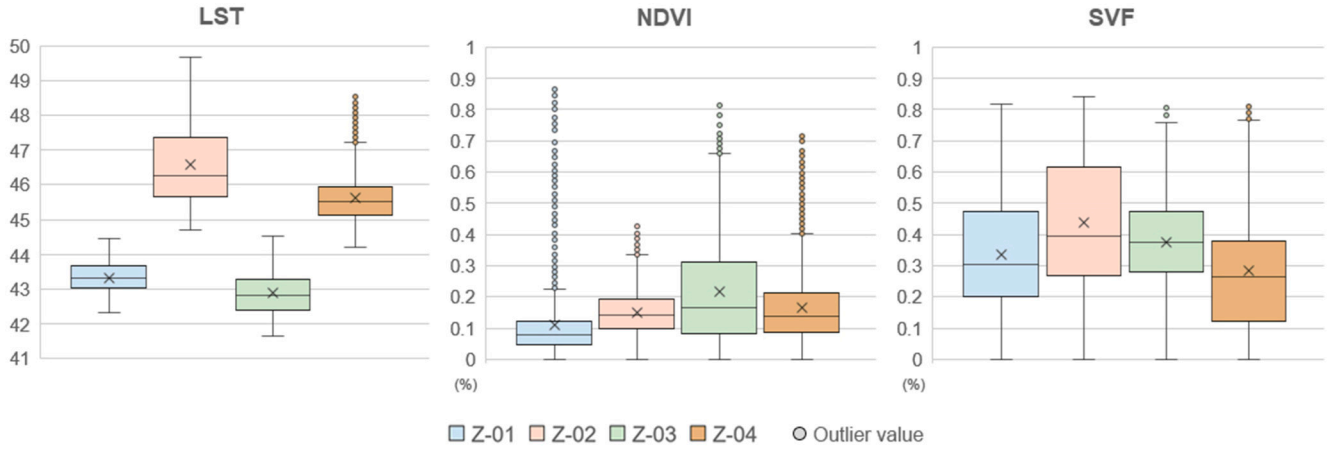


Figure 10. Quantitative assessment of the analyzed AOI's urban parameters.

Aligned with the above, the NDVI and the tree canopy cover also have a local relation at a fine scale with LST, not only due to sun exposure protection but also due to the cooling effects of green structures. This is clearly shown in the SVF heatmap (Figure 9). However, examining the SVF data distribution of Z-02 and Z-03 in Table 3, no great differences are observed. These zones, with different LCZ classifications, have similar SVF values due to the presence of vegetation. As a conclusion of this cross-assessment, a strong relation at the fine scale is observed between SVF and LST. Thus, greater urban compactness seems to result in lower diurnal temperatures.

Contrary to the previously discussed SVF-LST relation, Z-02 and Z-04 both have large open urban spaces with high SVF values (fourth column Figure 9). However, Z-02 reaches much higher LST in those (second column Figure 9). Both AOIs seem to have several previous soil areas according to the path in the first column of Figure 9; however, the difference is evident in the third column of Figure 9. The NDVI heatmap confirms a greater presence of active vegetation in Z-04, both in the tree canopy (related to the first column), and in green soils. High NDVI values indicate that the vegetation has enough quality and water access to still produce cooling effects, which is not the case in unbuilt areas of Z-02. This is also shown in the exposed areas of Z-03, which performs temperate LST, thanks to high NDVI values, as confirmed by Figure 10. These nuanced results highlight the importance of a multi-perspective at fine-scale analysis for such a complex reality. Only by cross-assessing multi-parameter data, it is possible to reach maximum information and accurate conclusions.

3.6. Study Limitations and Further Research

To conclude, some study limitations should be noted. Firstly, this method proposes a hybrid LCZ classification based on GIS parameters, expert knowledge and visually curated survey with satellite maps. Although it can become more time-consuming, this ensures the accuracy of the classification at a fine scale. However, future research should explore an automatic classification method based on geoprocessing that semi-automatically calculates urban parameters using GIS layers data and compares them with the LCZ classification, which will accelerate the process.

Furthermore, this research is based on indirect LST satellite acquisitions with an original image SR of 100 × 100 m. The literature and satellite providers ensure the quality of the obtained data for urban studies; however, it is important to note that these data are statistically resampled for representation purposes. The real urban environment highly depends on the properties of each material and tends to be sharper and more heterogeneous. Also, direct measurements (LST, AT, and others) will be necessary for subsequent investigations that focus more in-depth on the localized hot areas microclimate.

Another relevant aspect to note is that only one day of diurnal heat has been analyzed. It is well known that urban heat has a different behaviour during the day and night [19]. However, higher temperatures are reached during the day. This affects not only urban outdoor comfort but also indoor conditions and cooling energy consumption [5,89]. This is important to take into account when working on urban climate resilience. Some literature [6] focuses on UHI mitigation techniques, where high SVF areas are extremely beneficial due to their ability to release heat to the sky at night time. However, as this research has proved, there is also a notable relationship between SVF and diurnal heat exposure. As one of the main aims of research in urban climatic studies is to improve the lives of city residents, a holistic approach to urban heat must be taken. In this sense, further research should propose a balanced solution to mitigate heat during the daytime, but also allow it to be released during nighttime; that is maximizing the urban heat cycle mitigation [10].

In addition, once this methodology is established, further research should extend this approach to more cities with different climates, as the present research has focused only on one city, one climate case study. This could assess the methodology's capabilities in diverse climates and locations, which would provide a substantial climatic database. This could serve for further investigations, such as finding and comparing correlations between various urban parameters depending on the city's climate, thereby expanding the study's conclusions.

Finally, as the aim of this research is to conduct a straightforward analysis to identify hotspots in the city, it employs a low-resource and easily addressed methodology that allows for the identification of critical zones or areas of opportunity. Thus, this is not an exhaustive heat analysis but rather a diagnosis and identification of areas using the potential of remote sensing. However, once critical hotspots have already been located, more advanced spatiotemporal analysis methods would be necessary to significantly enhance the examination of the heat environment and its driving factors.

4. Conclusions

This paper provides an affordable GIS-based methodology, presented as a step-by-step guideline that analyses with a cross-assessment the urban heat. The main novelty of this study lies in presenting an easily approachable methodology that, based on a wealth of knowledge and previous studies, and using simple computational tools, all based on open data and software, can provide a solution for the rapid diagnosis and detection of hotspots in cities. Such contribution is important for urban thermal environment assessment, especially during prolonged heat waves and synergy with UHI phenomena to detect and measure urban thermal hotspots, graphically showing their location in the urban fabric. Furthermore, all this research has been developed based on standardized GIS open data information from official sources and can be processed on personal computers with free user-friendly software. This makes the guidelines accessible to designers and policymakers. Therefore, this methodology can be extrapolated and reproduced in most warm cities, constituting in itself a recommendation for urban sustainability policy and climate change mitigation, as it serves as a powerful tool for large-scale preliminary diagnosis.

The application of the methodology in the specific case study of Sevilla city has initially filled in relevant information on urban heat performance. In this case, differences in more than 10 °C in LST have been found within residential areas, while the city hotspots have been located and mapped, obtaining that 11% of the residential areas suffer a higher LST exposure. Moreover, it has been shown that the most extended urban fabric, LCZ-5 areas (Open midrise built type according to Stewart and Oke [27]), is more prone to suffer high heat exposure during the day. In addition, thanks to the fine spatial resolution, urban measurable parameters, such as compactness, SVF, vegetation and its quality or types of urban materials, have been found to be crucial to improving or worsening the diurnal thermal comfort of city inhabitants.

The combination of high-resolution thermal images with the simultaneous analysis of these diverse urban parameters has proved to be very useful in providing extensive knowledge of heat performance. This type of cross-assessment data allows a new preliminary approach that focuses on the diurnal heat, studied less than nocturnal heat, even if this produces the highest temperature and cooling energy demand peaks. Although this research has focused on this aspect, future studies should consider the whole day heat cycle performance in order to improve understanding of the city climates. Beyond the key limitation identified in the previous section, that could be addressed as future developments from this study. In this sense, it is necessary to optimize the satellite scanning frequency and mostly, the SR, with comparative day and night finer images, which can analyze the evolution of the city's thermal performance in different times and zones. However, this will depend on particular requests for a particular sweep of the satellites. Both the current and future results will optimize urban comfort and improve the energy efficiency of buildings.

The replicability of this methodology in other cities could provide a valuable first approach, making it possible to organize and prioritize more in-depth studies. This contributes to providing a useful and affordable diagnostic tool to detect vulnerable zones that can be converted into areas of opportunity for interventions. These aspects should be taken into account by public administrations when proposing future interventions or urban refurbishments, as this will help to guarantee more liveable urban spaces and improve the sustainability of cities against overheating hazards.

Author Contributions: Conceptualization, C.G.-M.; methodology, J.S.-C. and A.S.-J.; software, J.S.-C.; validation, A.S.-J. and C.R.-G.; formal analysis, J.S.-C.; investigation, J.S.-C. and A.S.-J.; resources, C.R.-G. and C.G.-M.; data curation, J.S.-C.; writing—original draft preparation, J.S.-C. and A.S.-J.; writing—review and editing, C.R.-G. and C.G.-M.; visualization, J.S.-C.; supervision, C.G.-M.; project administration, C.G.-M.; funding acquisition, C.R.-G. and C.G.-M. All authors have read and agreed to the published version of the manuscript.

Funding: This work has been supported by the project PID2021-124539OB-I00 funded by MICIU/AEI/10.13039/501100011033 and by "ERDF A way of making Europe", project TED2021-129347B-C21 funded by MICIU/AEI/10.13039/501100011033 and by the "European Union NextGenerationEU/PRTR"; and predoctoral contract granted to J.S.C (FPU21/02458).

Data Availability Statement: The original contributions presented in this study are included in the article. Further inquiries can be directed to the corresponding author.

Acknowledgments: The authors want to acknowledge USGS, NASA, and ESA-Copernicus for providing Landsat 9, LULC and thermal open-access images; also, to Catastro and Ayto. de Sevilla for providing open GIS data; AEMet, and the Ayuda de Internacionalización de Investigación IUACC-23 y VII P.P. US.

Conflicts of Interest: The authors declare no conflicts of interest.

Nomenclature and Abbreviations

AOI	Area of Interest	SDGs	Sustainable Development Goals
AT	Air Temperature	SR	Spatial Resolution
ESA	European Space Agency	SUHI	Surface Urban Heat Island
GIS	Geographical Information System	SVF	Sky View Factor
LCZ	Local Climate Zone	SVQ	Seville
LST	Land Surface Temperature	TIRS	Thermal Infrared Sensor
LULC	Land Use–Land Cover	UHI	Urban Heat Island
NDVI	Normalized Difference Vegetation Index	UCI	Urban Cooling Island
RH	Relative Humidity	UN	United Nations

Appendix A.

Appendix A.1. Seville's Climate

The following images show the statistical annual hourly chart developed with the last available official registers (2007–2021). The main climate parameters related to LST are expressed as follows: AT in °C (Figure A1) and global radiation in W·h/m^2 (Figure A2).

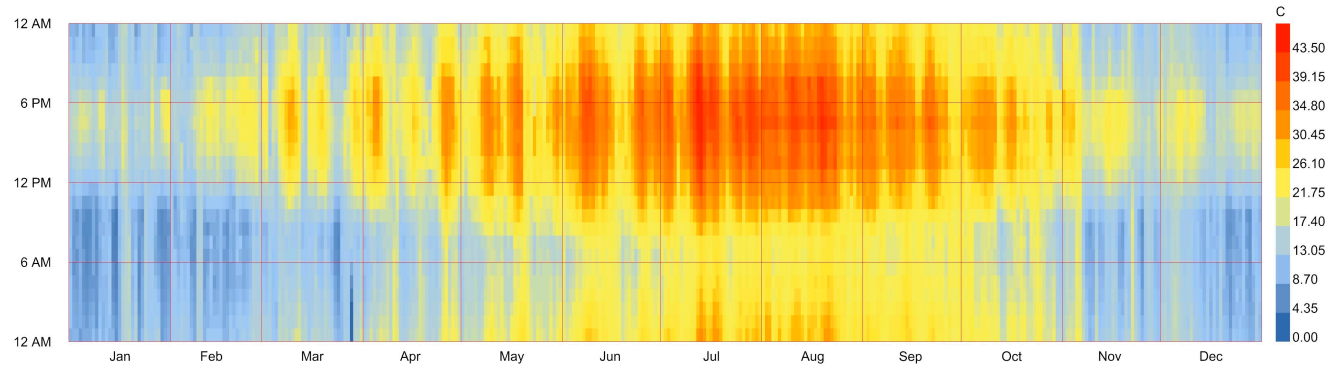


Figure A1. Annual hourly chart of air temperature (°C).

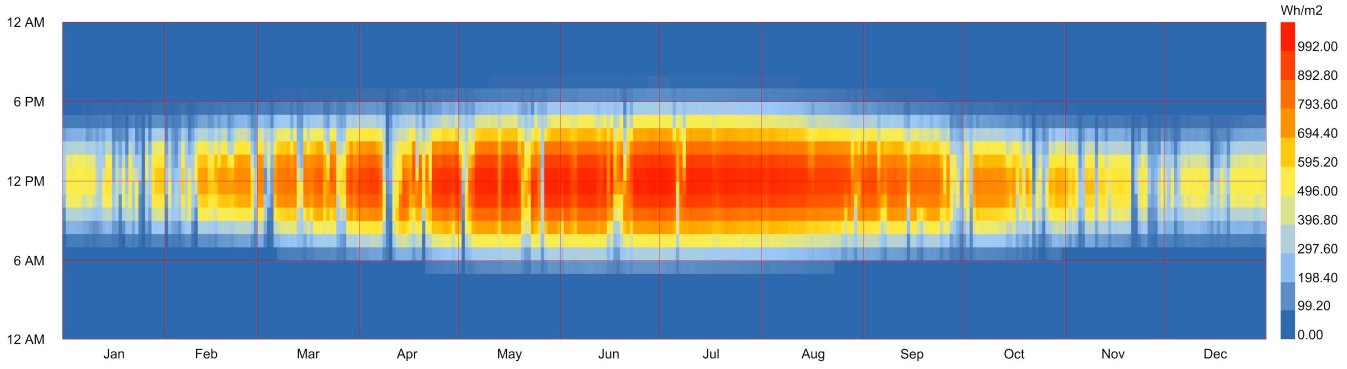


Figure A2. Annual hourly chart of direct solar radiation (W·h/m^2).

Appendix A.2. Studied Day Recorded Climate

The climate during the analyzed day was recorded by an own weather station, placed in the city. Air temperature and global horizontal radiation are shown in Figure A3.

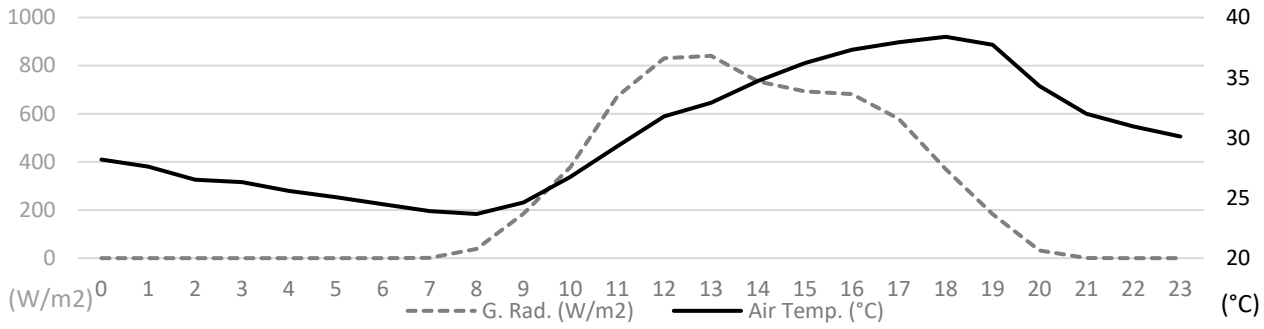


Figure A3. Hourly air temperature and global radiation in Seville 29 August 2023, measured by an own meteorological station in the city.

References

1. IPCC. Fifth Assessment Report. In *Climate Change 2014*; IPCC: Geneva, Switzerland, 2014.
2. IPCC. *Climate Change 2022: Impacts, Adaptation and Vulnerability*; IPCC: Geneva, Switzerland, 2022.
3. Ritchie, H.; Rodés-Guirao, L.; Mathieu, E.; Gerber, M.; Ortiz-Ospina, E.; Hasell, J.; Roser, M. Population Growth. 2023. Available online: https://ourworldindata.org/population-growth#article-citation (accessed on 18 December 2023).
4. The 17 Goals | Sustainable Development. Available online: https://sdgs.un.org/goals (accessed on 18 December 2023).
5. Santamouris, M.; Paolini, R.; Haddad, S.; Synnefa, A.; Garshasbi, S.; Hatvani-Kovacs, G.; Gobakis, K.; Yenneti, K.; Vasilakopoulou, K.; Feng, J. Heat mitigation technologies can improve sustainability in cities. An holistic experimental and numerical impact assessment of urban overheating and related heat mitigation strategies on energy consumption, indoor comfort, vulnerability and heat-related mortality and morbidity in cities. *Energy Build.* **2020**, *217*, 110002. [CrossRef]
6. Salata, F.; Golasi, I.; Petitti, D.; Vollaro, E.d.L.; Coppi, M.; Vollaro, A.d.L. Relating microclimate, human thermal comfort and health during heat waves: An analysis of heat island mitigation strategies through a case study in an urban outdoor environment. *Sustain. Cities Soc.* **2017**, *30*, 79–96. [CrossRef]
7. Kandelan, S.N.; Yeganeh, M.; Peyman, S.; Panchabikesan, K.; Eicker, U. Environmental study on greenery planning scenarios to improve the air quality in urban canyons. *Sustain. Cities Soc.* **2022**, *83*, 103993. [CrossRef]
8. Goldberg, V.; Kurbjuhn, C.; Bernhofer, C. How relevant is urban planning for the thermal comfort of pedestrians? Numerical case studies in two districts of the City of Dresden. *Meteorol. Z.* **2013**, *22*, 739–751. [CrossRef]
9. Kim, S.W.; Brown, R.D. Urban heat island (UHI) intensity and magnitude estimations: A systematic literature review. *Sci. Total Environ.* **2021**, *779*, 146389. [CrossRef]
10. Stewart, I.D.; Krayenhoff, E.S.; Voogt, J.A.; Lachapelle, J.A.; Allen, M.A.; Broadbent, A.M. Time Evolution of the Surface Urban Heat Island. *Earths Future* **2021**, *9*, e2021EF002178. [CrossRef]
11. García, D.H.; Díaz, J.A. Modeling of the Urban Heat Island on local climatic zones of a city using Sentinel 3 images: Urban determining factors. *Urban Clim.* **2021**, *37*, 100840. [CrossRef]
12. Lizana, J.; Núñez-Peiró, M.; Khosla, R.; Mcculloch, M. Citizen Data for Global Mapping of Atmospheric Urban Heat Islands 2023. Available online: https://doi.org/10.21203/rs.3.rs-2924752/v1 (accessed on 22 December 2023).
13. Núñez Peiró, M.; Sánchez-Guevara Sánchez, C.; Neila González, F.J. Update of the Urban Heat Island of Madrid and Its Influence on the Building's Energy Simulation. In *Sustainable Development and Renovation in Architecture, Urbanism and Engineering*; Springer International Publishing: Cham, Switzerland, 2017; pp. 339–350. [CrossRef]
14. Rodríguez, L.R.; Ramos, J.S.; de la Flor, F.J.S.; Domínguez, S. Analyzing the urban heat Island: Comprehensive methodology for data gathering and optimal design of mobile transects. *Sustain. Cities Soc.* **2020**, *55*, 102027. [CrossRef]
15. Oke, T.R. *Boundary Layer Climates*; Methuen: Methuen, MA, USA, 1978.
16. Oke, T.R. The distinction between canopy and boundary-layer urban heat islands. *Atmosphere* **1976**, *14*, 268–277. [CrossRef]
17. Martin, M.; Chong, A.; Biljecki, F.; Miller, C. Infrared thermography in the built environment: A multi-scale review. *Renew. Sustain. Energy Rev.* **2022**, *165*, 112540. [CrossRef]
18. Voogt, J.A.; Oke, T.R. Thermal remote sensing of urban climates. *Remote Sens. Env.* **2003**, *86*, 370–384. [CrossRef]
19. Oke, T.R.; Mills, G.; Christen, A.; Voogt, J. *Urban Climates*; Cambridge University Press: Cambridge, UK, 2017. [CrossRef]
20. Scolio, M.; Kremer, P.; Zhang, Y.; Shakya, K.M. Spatial-temporal modeling of the relationship between surface temperature and air temperature in metropolitan urban systems. *Urban Clim.* **2024**, *55*, 101921. [CrossRef]
21. Mihăilă, D.; Bistricean, P.I.; Sfîcă, L.; Horodnic, V.D.; Prisăcariu, A.; Amihăesei, V.A. Summer Discrepancies Between 2 m Air Temperature and Landsat LST in Suceava City, Northeastern Romania. *Remote Sens.* **2024**, *16*, 2967. [CrossRef]

22. Schaefer, M.; Salari, H.E.; Köckler, H.; Thinh, N.X. Assessing local heat stress and air quality with the use of remote sensing and pedestrian perception in urban microclimate simulations. *Sci. Total Environ.* **2021**, *794*, 148709. [CrossRef]
23. Mushore, T.D.; Odindi, J.; Slotow, R.; Mutanga, O. Remote Sensing-Based Outdoor Thermal Comfort Assessment in Local Climate Zones in the Rural–Urban Continuum of eThekwini Municipality, South Africa. *Remote Sens.* **2023**, *15*, 5461. [CrossRef] [PubMed]
24. U.S. Geological Survey. Landsat 9. Available online: https://www.usgs.gov/landsat-missions/landsat-9 (accessed on 30 November 2023).
25. Wang, M.; Li, M.; Zhang, Z.; Hu, T.; He, G.; Zhang, Z.; Wang, G.; Li, H.; Tan, J.; Liu, X. Land Surface Temperature Retrieval from Landsat 9 TIRS-2 Data Using Radiance-Based Split-Window Algorithm. *IEEE J. Sel. Top. Appl. Earth Obs. Remote. Sens.* **2023**, *16*, 1100–1112. [CrossRef]
26. Oke, T.R. Canyon geometry and the nocturnal urban heat island: Comparison of scale model and field observations. *J. Climatol.* **1981**, *1*, 237–254. [CrossRef]
27. Stewart, I.D.; Oke, T.R. Local Climate Zones for Urban Temperature Studies. *Bull. Am. Meteorol. Soc.* **2012**, *93*, 1879–1900. [CrossRef]
28. Fernandes, R.; Nascimento, V.; Freitas, M.; Ometto, J. Local Climate Zones to Identify Surface Urban Heat Islands: A Systematic Review. *Remote Sens.* **2023**, *15*, 884. [CrossRef]
29. Badaro-Saliba, N.; Adjizian-Gerard, J.; Zaarour, R.; Najjar, G. LCZ scheme for assessing Urban Heat Island intensity in a complex urban area (Beirut, Lebanon). *Urban Clim.* **2021**, *37*, 100846. [CrossRef]
30. Žgela, M.; Herceg-Bulić, I.; Lozuk, J.; Jureša, P. Linking land surface temperature and local climate zones in nine Croatian cities. *Urban Clim.* **2024**, *54*, 101842. [CrossRef]
31. Li, N.; Wang, B.; Yao, Y.; Chen, L.; Zhang, Z. Thermal Contribution of the Local Climate Zone and Its Spatial Distribution Effect on Land Surface Temperature in Different Macroclimate Cities. *Remote Sens.* **2022**, *14*, 4029. [CrossRef]
32. Hadavi, M.; Pasdarshahri, H. Investigating effects of urban configuration and density on urban climate and building systems energy consumption. *J. Build. Eng.* **2021**, *44*, 102710. [CrossRef]
33. Maiullari, D.; Gherri, B.; Finizza, C.; Maretto, M.; Naboni, E. Climate change and indoor temperature variation in Venetian buildings: The role of density and urban form. *J. Phys. Conf. Ser.* **2021**, *2042*, 012060. [CrossRef]
34. Rao, P.; Tassinari, P.; Torreggiani, D. Exploring the land-use urban heat island nexus under climate change conditions using machine learning approach: A spatio-temporal analysis of remotely sensed data. *Heliyon* **2023**, *9*, e18423. [CrossRef] [PubMed]
35. He, B.-J.; Zhao, Z.-Q.; Shen, L.-D.; Wang, H.-B.; Li, L.-G. An approach to examining performances of cool/hot sources in mitigating/enhancing land surface temperature under different temperature backgrounds based on landsat 8 image. *Sustain. Cities Soc.* **2019**, *44*, 416–427. [CrossRef]
36. Zhao, Z.-Q.; He, B.-J.; Li, L.-G.; Wang, H.-B.; Darko, A. Profile and concentric zonal analysis of relationships between land use/land cover and land surface temperature: Case study of Shenyang, China. *Energy Build.* **2017**, *155*, 282–295. [CrossRef]
37. Copernicus Land Monitoring Service. CORINE Land Cover. Available online: https://land.copernicus.eu/en/products/corine-land-cover (accessed on 29 July 2024).
38. Maiullari, D.; Esch, M.P.-V.; Van Timmeren, A. A Quantitative Morphological Method for Mapping Local Climate Types. *Urban Plan.* **2021**, *6*, 240–257. [CrossRef]
39. Salvati, A.; Monti, P.; Roura, H.C.; Cecere, C. Climatic performance of urban textures: Analysis tools for a Mediterranean urban context. *Energy Build.* **2019**, *185*, 162–179. [CrossRef]
40. Dirksen, M.; Ronda, R.J.; Theeuwes, N.E.; Pagani, G.A. Sky view factor calculations and its application in urban heat island studies. *Urban Clim.* **2019**, *30*, 100498. [CrossRef]
41. Diz-Mellado, E.; López-Cabeza, V.P.; Roa-Fernández, J.; Rivera-Gómez, C.; Galán-Marín, C. Energy-saving and thermal comfort potential of vernacular urban block porosity shading. *Sustain. Cities Soc.* **2023**, *89*, 104325. [CrossRef]
42. Chen, Q.; Cheng, Q.; Chen, Y.; Li, K.; Wang, D.; Cao, S. The Influence of Sky View Factor on Daytime and Nighttime Urban Land Surface Temperature in Different Spatial-Temporal Scales: A Case Study of Beijing. *Remote Sens.* **2021**, *13*, 4117. [CrossRef]
43. Huete, A.; Didan, K.; Miura, T.; Rodriguez, E.P.; Gao, X.; Ferreira, L.G. Overview of the radiometric and biophysical performance of the MODIS vegetation indices. *Remote Sens. Environ.* **2002**, *83*, 195–213. [CrossRef]
44. Rouse, J.W., Jr.; Haas, R.H.; Schell, J.A.; Deering, D.W. *Monitoring Vegetation Systems in the Great Plains with ERTS*; NASA. Goddard Space Flight Center 3d ERTS-1 Symp.: Washington, DC, USA, 1974; Volume 1, Section A.
45. Sola-Caraballo, J.; Lopez-Cabeza, V.P.; Roa-Fernández, J.; Rivera-Gomez, C.; Galan-Marin, C. Assessing and upgrading urban thermal resilience of a Spanish MoMo neighbourhood over the span of 1960–2080. *Build. Environ.* **2024**, *256*, 111485. [CrossRef]
46. Marković, M.; Cheema, J.; Teofilović, A.; Čepić, S.; Popović, Z.; Tomićević-Dubljević, J.; Pause, M. Monitoring of Spatiotemporal Change of Green Spaces in Relation to the Land Surface Temperature: A Case Study of Belgrade, Serbia. *Remote Sens.* **2021**, *13*, 3846. [CrossRef]

47. Serrano-Jiménez, A.; Díaz-López, C.; Ramírez-Juidias, E.; Barrios-Padura, Á. Multi-criteria assessment model on environmental ergonomics for decision-making in schoolyards based on remote-sensing and GIS resources. *Sustain. Cities Soc.* **2023**, *92*, 104481. [CrossRef]
48. OSGeo. QGIS Project. Available online: https://qgis.org/en/site/index.html (accessed on 30 November 2023).
49. Fabbri, K.; Zuppiroli, M.; Ambrogio, K. Heritage buildings and energy performance: Mapping with GIS tools. *Energy Build.* **2012**, *48*, 137–145. [CrossRef]
50. Ahmed, S. Assessment of urban heat islands and impact of climate change on socioeconomic over Suez Governorate using remote sensing and GIS techniques. *Egypt. J. Remote Sens. Space Sci.* **2018**, *21*, 15–25. [CrossRef]
51. Serrano-Jiménez, A.; Hiruelo-Pérez, J.; Ramírez-Juidias, E.; Barrios-Padura, Á. Identifying design shortcomings and heat-island effects in schools located in warm climates: An outdoor environmental assessment procedure based on remote sensing tools. *J. Build. Eng.* **2021**, *43*, 103209. [CrossRef]
52. Sangiorgio, V.; Capolupo, A.; Tarantino, E.; Fiorito, F.; Santamouris, M. Evaluation of Absolute Maximum Urban Heat Island Intensity Based on a Simplified Remote Sensing Approach. *Environ. Eng. Sci.* **2022**, *39*, 296–307. [CrossRef]
53. López-Moreno, H.; Núñez-Peiró, M.; Sánchez-Guevara, C.; Neila, J. On the identification of Homogeneous Urban Zones for the residential buildings' energy evaluation. *Build. Environ.* **2022**, *207*, 108451. [CrossRef]
54. Sola-Caraballo, J.; Serrano-Jiménez, A.; Rivera-Gomez, C.; Galan-Marin, C. GIS-Based Remote Sensing Approach for Urban Studies: Locating and Mapping Vulnerable Areas in Hot Climates. In Proceedings of the 37th PLEA Conference, Wrocław, Poland, 25–28 June 2024; Sustainable Architecture and Urban Design: Wroclaw, Poland, 2024; pp. 106–111.
55. Ullah, W.; Ahmad, K.; Ullah, S.; Tahir, A.A.; Javed, M.F.; Nazir, A.; Abbasi, A.M.; Aziz, M.; Mohamed, A. Analysis of the relationship among land surface temperature (LST), land use land cover (LULC), and normalized difference vegetation index (NDVI) with topographic elements in the lower Himalayan region. *Heliyon* **2023**, *9*, e13322. [CrossRef] [PubMed]
56. Coutts, A.M.; Harris, R.J.; Phan, T.; Livesley, S.J.; Williams, N.S.G.; Tapper, N.J. Thermal infrared remote sensing of urban heat: Hotspots, vegetation, and an assessment of techniques for use in urban planning. *Remote Sens. Environ.* **2016**, *186*, 637–651. [CrossRef]
57. Guerri, G.; Crisci, A.; Messeri, A.; Congedo, L.; Munafò, M.; Morabito, M. Thermal Summer Diurnal Hot-Spot Analysis: The Role of Local Urban Features Layers. *Remote Sens.* **2021**, *13*, 538. [CrossRef]
58. Brousse, O.; Martilli, A.; Foley, M.; Mills, G.; Bechtel, B. Wudapt, an efficient land use producing data tool for mesoscale models? Integration of urban LCZ in WRF over Madrid. *Urban Clim.* **2016**, *17*, 116–134. [CrossRef]
59. Jumari, N.A.S.K.; Ahmed, A.N.; Huang, Y.F.; Ng, J.L.; Koo, C.H.; Chong, K.L.; Sherif, M.; Elshafie, A. Analysis of urban heat islands with landsat satellite images and GIS in Kuala Lumpur Metropolitan City. *Heliyon* **2023**, *9*, e18424. [CrossRef]
60. Hidalgo-García, D.; Arco-Díaz, J. Modeling the Surface Urban Heat Island (SUHI) to study of its relationship with variations in the thermal field and with the indices of land use in the metropolitan area of Granada (Spain). *Sustain. Cities Soc.* **2022**, *87*, 104166. [CrossRef]
61. Sharmin, T.; Steemers, K.; Matzarakis, A. Microclimatic modelling in assessing the impact of urban geometry on urban thermal environment. *Sustain. Cities Soc.* **2017**, *34*, 293–308. [CrossRef]
62. OneBuilding. Available online: https://climate.onebuilding.org (accessed on 30 March 2024).
63. de Meteorología, A.E. AEMet. Observación. Available online: https://www.aemet.es/es/eltiempo/observacion/ultimosdatos (accessed on 9 January 2024).
64. U.S. Geological Survey. Landsat Acquisition | Landsat Missions. Available online: https://landsat.usgs.gov/landsat_acq (accessed on 30 November 2023).
65. Sede Electrónica del Catastro—Difusión de Datos Catastrales. Available online: https://www.sedecatastro.gob.es/Accesos/SECAccDescargaDatos.aspx (accessed on 30 November 2023).
66. EOS Data Analytics. Crop Monitoring: Farm Software For Agricultural Sector. Available online: https://eos.com/products/crop-monitoring/ (accessed on 15 December 2023).
67. Köppen, W. Das Geographische System der Klimate. (Berlin, 1936). Available online: https://commons.wikimedia.org/wiki/File:Das_geographische_System_der_Klimate_(1936).pdf (accessed on 28 November 2023).
68. Lee, T.W.; Lee, J.Y.; Wang, Z.H. Scaling of the urban heat island intensity using time-dependent energy balance. *Urban Clim.* **2012**, *2*, 16–24. [CrossRef]
69. U.S. Geological Survey. EarthExplorer. Available online: https://earthexplorer.usgs.gov/ (accessed on 30 November 2023).
70. U.S. Geological Survey. Landsat 8-9 Collection 2 Level 2 Science Product Guide. Available online: https://www.usgs.gov/media/files/landsat-8-9-collection-2-level-2-science-product-guide (accessed on 30 November 2023).
71. OpenStreetMap. Available online: https://www.openstreetmap.org/ (accessed on 15 December 2023).
72. Takeda, H.; Farsiu, S.; Milanfar, P. Kernel regression for image processing and reconstruction. *IEEE Trans. Image Process.* **2007**, *16*, 349–366. [CrossRef] [PubMed]

73. Barnsley, M.J.; Barr, S.L. Inferring urban land use from satellite sensor images using Kernel-based spatial reclassification. *Photogramm. Eng. Remote Sens.* **1996**, *62*, 949–958.
74. Doulos, L.; Santamouris, M.; Livada, I. Passive cooling of outdoor urban spaces. The role of materials. *Sol. Energy* **2004**, *77*, 231–249. [CrossRef]
75. Demuzere, M.; Kittner, J.; Bechtel, B. LCZ Generator: A Web Application to Create Local Climate Zone Maps. *Front. Environ. Sci.* **2021**, *9*, 637455. [CrossRef]
76. Huang, F.; Jiang, S.; Zhan, W.; Bechtel, B.; Liu, Z.; Demuzere, M. Mapping local climate zones for cities: A large review. *Remote Sens. Environ.* **2023**, *292*, 113573. [CrossRef]
77. Submitted LCZ Maps n.d. Available online: https://lcz-generator.rub.de/submissions (accessed on 22 December 2024).
78. Stewart, I.; Oke, T. Classifying urban climate field sites by "local climate zones": The case of Nagano, Japan. In Proceedings of the 7th International Conference on Urban Climate, Yokohama, Japan, 29 June–3 July 2009.
79. Dogan, T.; Samaranayake, S.; Saraf, N. Urbano: A New Tool to Promote Mobility-Aware Urban Design, Active Transportation Modeling and Access Analysis for Amenities and Public Transport. In Proceedings of the Symposium on Simulation for Architecture and Urban Design, Delft, The Netherlands, 4–7 June 2018; pp. 1–8. Available online: https://www.simaud.org/ (accessed on 22 November 2023).
80. Sadeghipour Roudsari, M.; Mackey, C. Ladybug Tools 2013. Available online: https://www.ladybug.tools/ (accessed on 22 November 2023).
81. OECD. Urban Population by City Size (Indicator). OECD. 2023. Available online: https://www.oecd-ilibrary.org/urban-rural-and-regional-development/urban-population-by-city-size/indicator/english_b4332f92-en (accessed on 20 December 2023).
82. Andrade, C.; Contente, J. Köppen's climate classification projections for the Iberian Peninsula. *Clim. Res.* **2020**, *81*, 71–89. [CrossRef]
83. ESA. ESA—Top 10 Earth Observation Stories of 2023. 2023. Available online: https://www.esa.int/Applications/Observing_the_Earth/Top_10_Earth_observation_stories_of_2023 (accessed on 22 November 2024).
84. Google LLC. Google Earth n.d. Available online: https://earth.google.com/web/ (accessed on 18 November 2023).
85. Santamouris, M.; Gaitani, N.; Spanou, A.; Saliari, M.; Giannopoulou, K.; Vasilakopoulou, K.; Kardomateas, T. Using cool paving materials to improve microclimate of urban areas—Design realization and results of the flisvos project. *Build. Environ.* **2012**, *53*, 128–136. [CrossRef]
86. Namazi, Y.; Charlesworth, S.; Montazami, A.; Taleghani, M. The impact of local microclimates and Urban Greening Factor on schools' thermal conditions during summer: A study in Coventry, UK. *Build Environ.* **2024**, *262*, 111793. [CrossRef]
87. Parison, S.; Chaumont, M.; Kounkou-Arnaud, R.; Long, F.; Bernik, A.; Da Silva, M.; Hendel, M. The Effects of Greening a Parking Lot as a Heat Mitigation Strategy on Outdoor Thermal Stress Using Fixed and Mobile Measurements: Case-Study Project "Tertiary Forest". *Sustain. Cities Soc.* **2023**, *98*, 104818. [CrossRef]
88. Sola-Caraballo, J.; Lopez-Cabeza, V.P.; Roa-Fernandez, J.; Rivera-Gomez, C.; Palomares-Figueres, M.T.; Galan-Marin, C. Assessing the microclimatic adaptation of a Modern Movement 1960s neighbourhood through its urban evolution. In Proceedings of the 18th IBPSA International Conference, Shanghai, China, 4–6 September 2023. [CrossRef]
89. Brozovsky, J.; Radivojevic, J.; Simonsen, A. Assessing the impact of urban microclimate on building energy demand by coupling CFD and building performance simulation. *J. Build. Eng.* **2022**, *55*, 104681. [CrossRef]

Disclaimer/Publisher's Note: The statements, opinions and data contained in all publications are solely those of the individual author(s) and contributor(s) and not of MDPI and/or the editor(s). MDPI and/or the editor(s) disclaim responsibility for any injury to people or property resulting from any ideas, methods, instructions or products referred to in the content.